The Astrophysical Journal, 940:68 (13pp), 2022 November 20
https://doi.org/10.3847/1538-4357/ac9978

Constraints on the Optical Depth to Reionization from Balloon-borne Cosmic Microwave Background Measurements

Josquin Errard[1], Mathieu Remazeilles[2,3], Jonathan Aumont[4], Jacques Delabrouille[5], Daniel Green[6], Shaul Hanany[7], Brandon S. Hensley[8], and Alan Kogut[9]






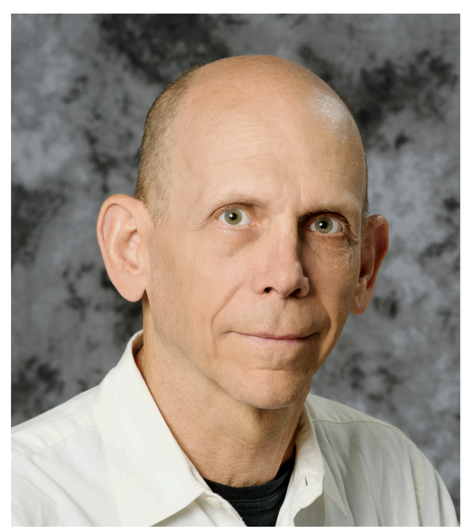

Josquin Errard, APC (CNRS)
CoPhy, LPNHE, January 2023

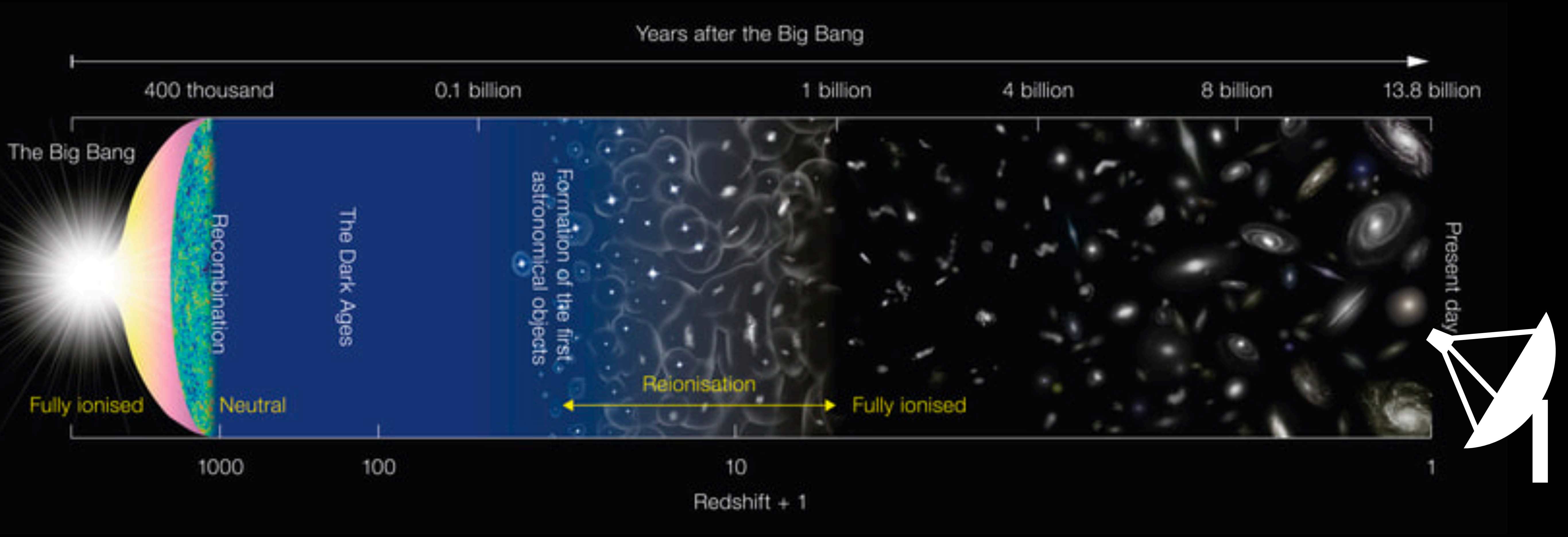

Josquin Errard, APC (CNRS)
Errard, Remazeilles et al. (ApJ, 2022)
CoPy, LPNHE, January 2023

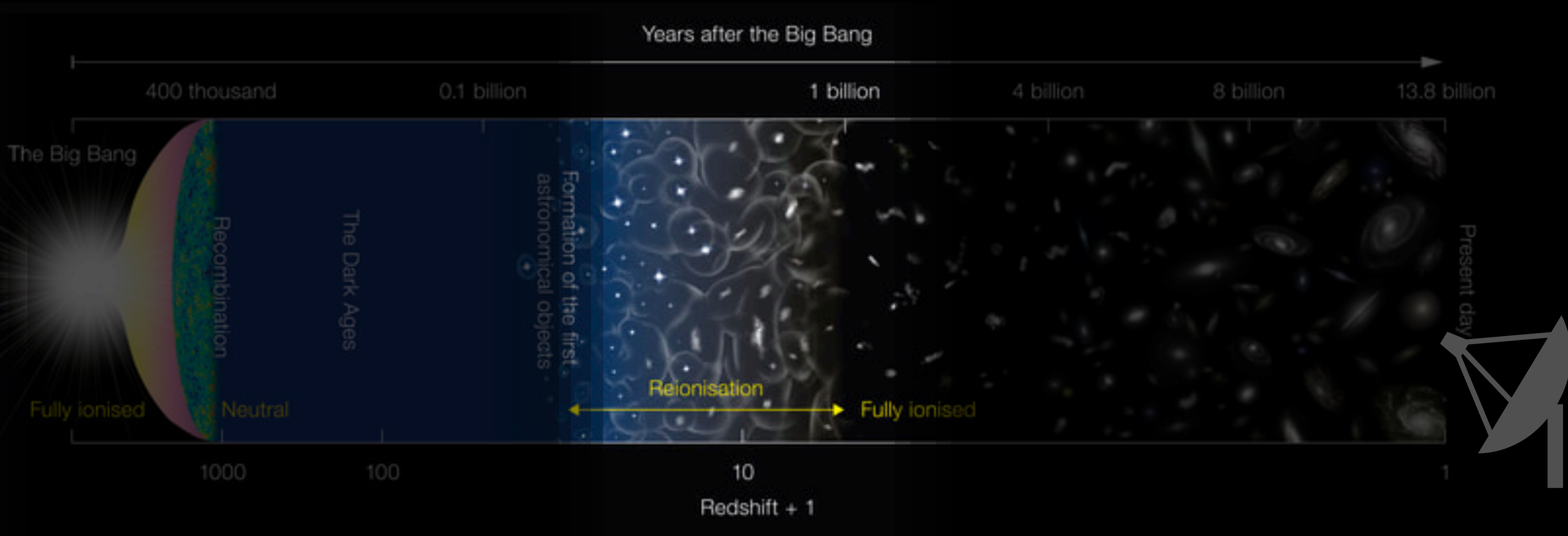

Josquin Errard, APC (CNRS)
Errard, Remazeilles et al. (ApJ, 2022)
CoPy, LPNHE, January 2023

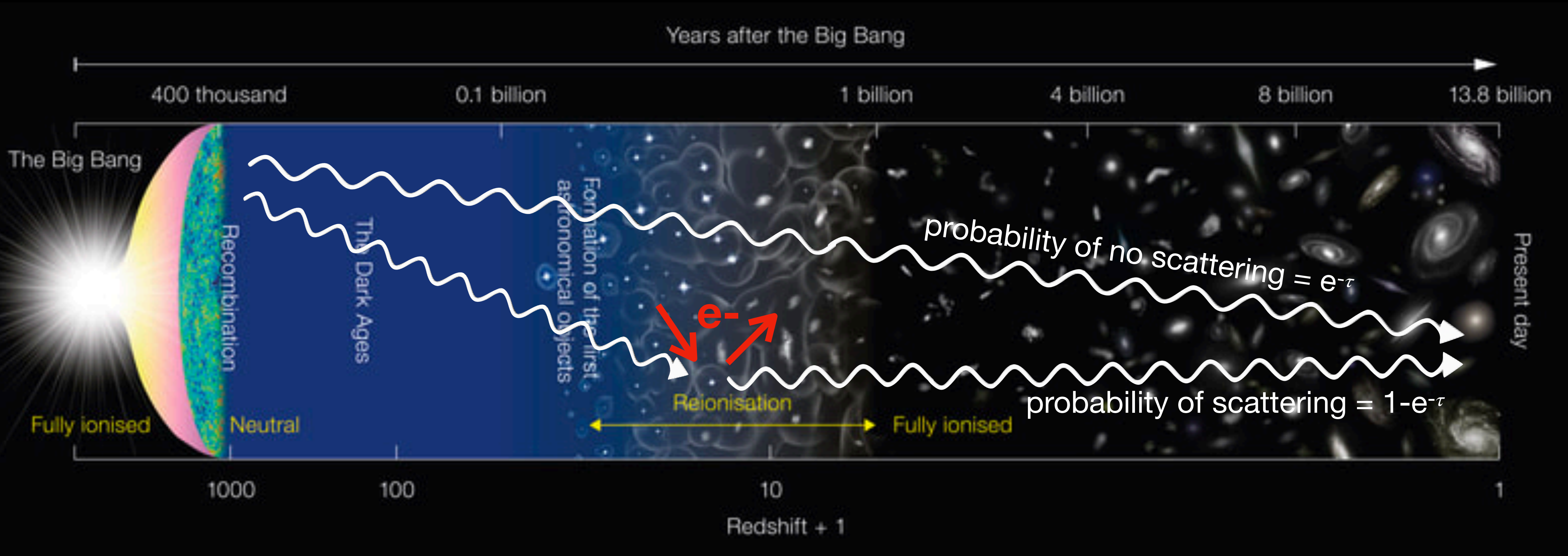

Years after the Big Bang
400 thousand
0.1 billion
1 billion
4 billion
8 billion
13.8 billion
The Big Bang
Recombination
The Dark Ages
Formation of the first astronomical objects
probability of no scattering = $e^{-\tau}$
e-
Present day
Reionisation
probability of scattering = $1-e^{-\tau}$
Fully ionised
Neutral
Fully ionised
1000
100
10
1
Redshift + 1

details of the reionization process and
thus to the history of structure formation

$$\tau = n_{\rm H}(0) c \sigma_{\rm T} \int_0^{z_{\rm max}} dz\, x_{\rm e}(z) \frac{(1+z)^2}{H(z)}$$

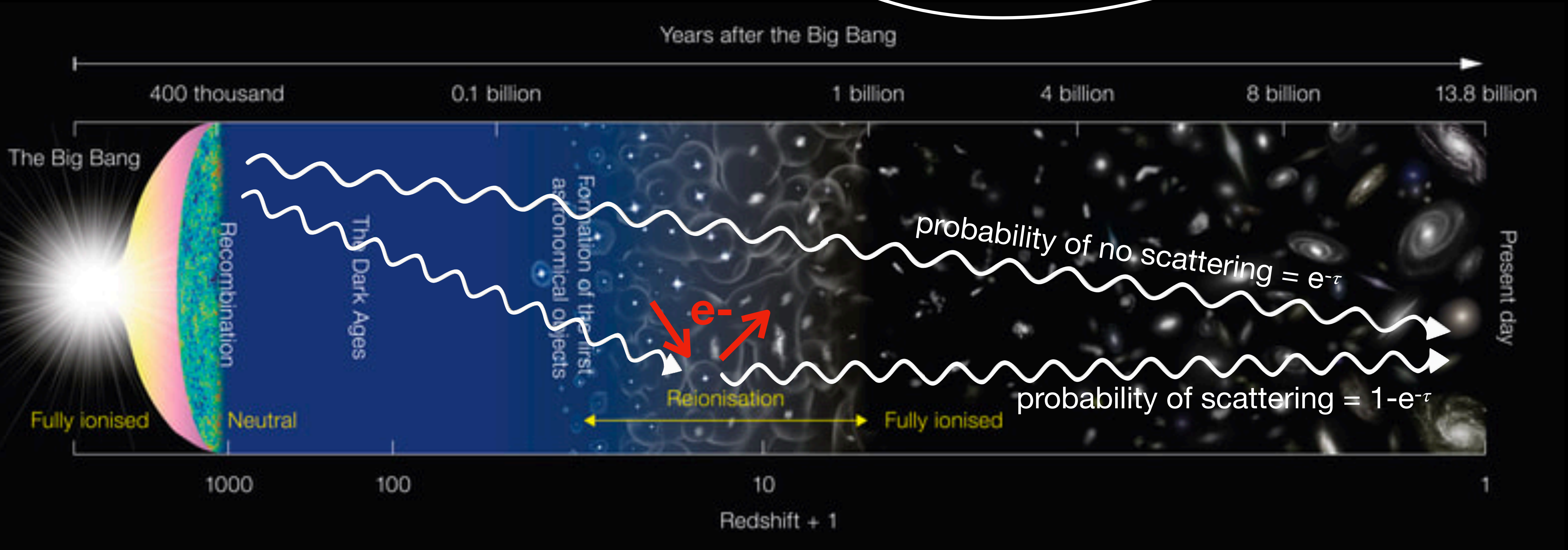

details of the reionization process and thus to the history of structure formation

$$\tau = n_{\rm H}(0) c \sigma_{\rm T} \int_0^{z_{\rm max}} dz\, x_{\rm e}(z) \frac{(1+z)^2}{H(z)}$$

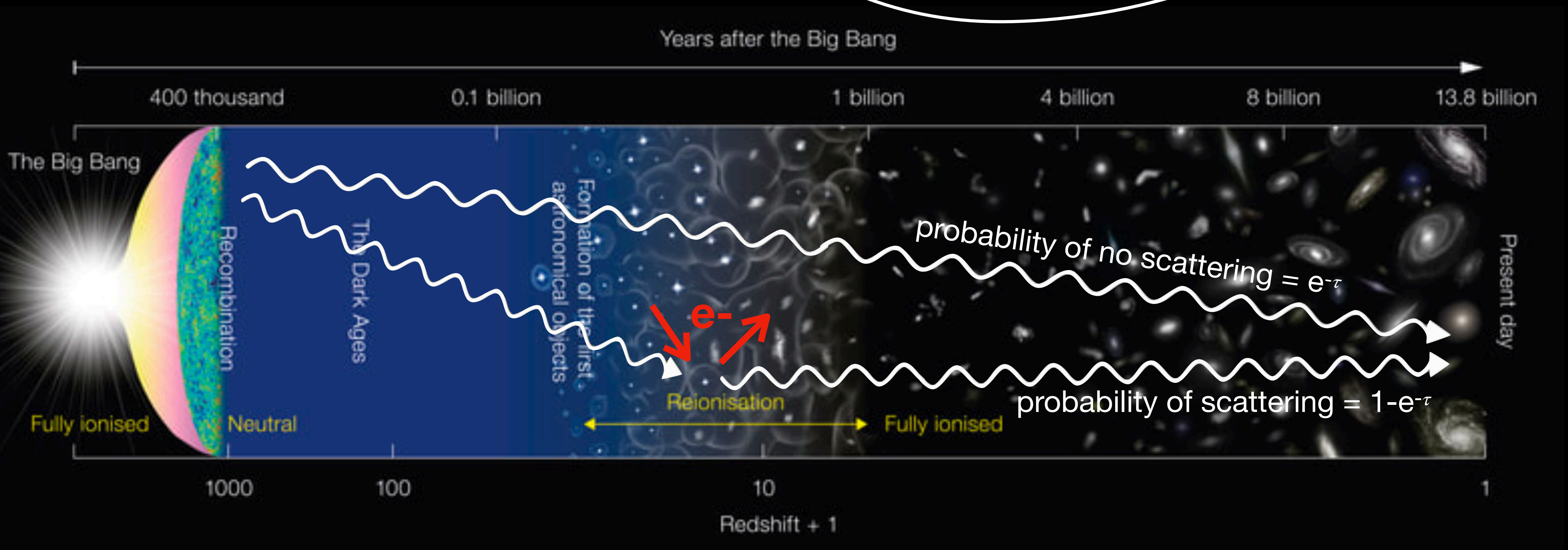

- **Astrophysical** interest
  - Sources producing the ionizing photons (early star-forming galaxies or exotic sources)?
  - Mean free path of the ionizing photons / typical opacity of the intergalactic medium ?
  - Efficiency of the UV photons production?
  - Duration of the reionization epoch?
- **Cosmology: (Thomson scattering optical depth τ) error propagates to other cosmological parameters**
  - leading source of error for neutrino mass as characterized from gravitational lensing
  - growth of structure and cosmic acceleration [Hu & Jain 04]

details of the reionization process and thus to the history of structure formation

$$\tau = n_{\mathrm{H}}(0) c \sigma_{\mathrm{T}} \int_0^{z_{\max}} dz\, x_e(z) \frac{(1+z)^2}{H(z)}$$

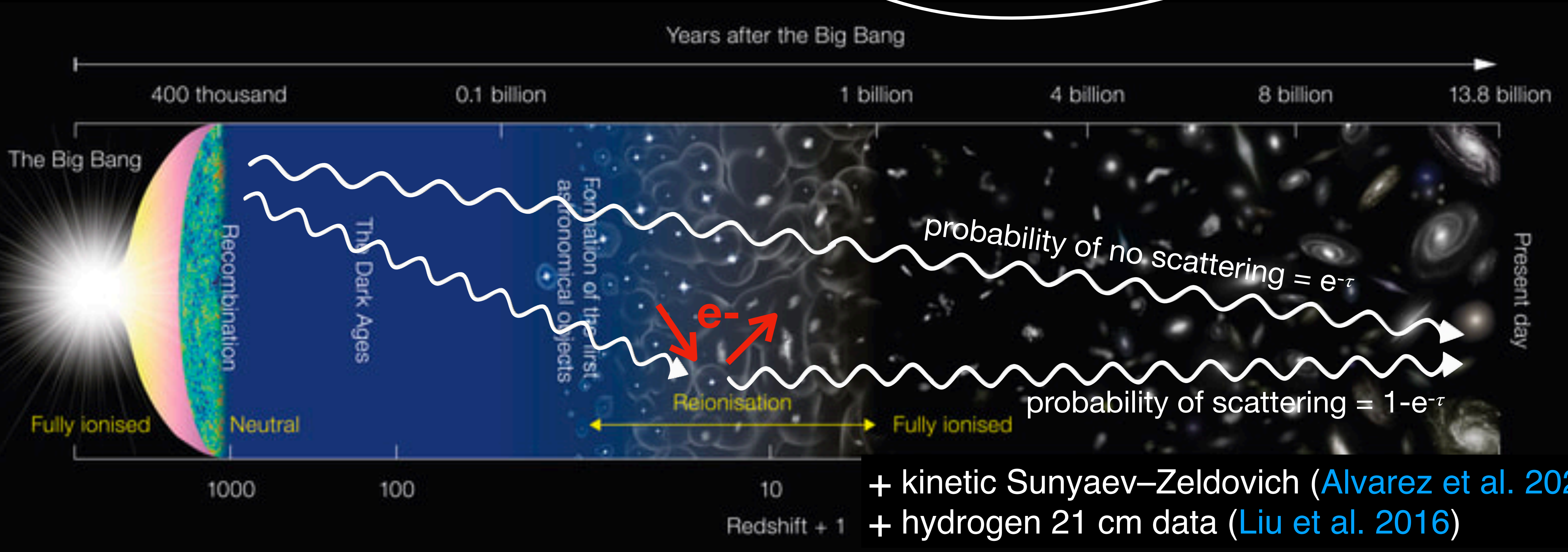

+ kinetic Sunyaev–Zeldovich (Alvarez et al. 2021)
+ hydrogen 21 cm data (Liu et al. 2016)

- **Astrophysical** interest
  - Sources producing the ionizing photons (early star-forming galaxies or exotic sources)?
  - Mean free path of the ionizing photons / typical opacity of the intergalactic medium ?
  - Efficiency of the UV photons production?
  - Duration of the reionization epoch?
- **Cosmology: (Thomson scattering optical depth τ) error propagates to other cosmological parameters**
  - leading source of error for neutrino mass as characterized from gravitational lensing
  - growth of structure and cosmic acceleration [Hu & Jain 04]

details of the reionization process and thus to the history of structure formation

$$\tau = n_{\rm H}(0) c \sigma_{\rm T} \int_0^{z_{\rm max}} dz\, x_{\rm e}(z) \frac{(1+z)^2}{H(z)}$$

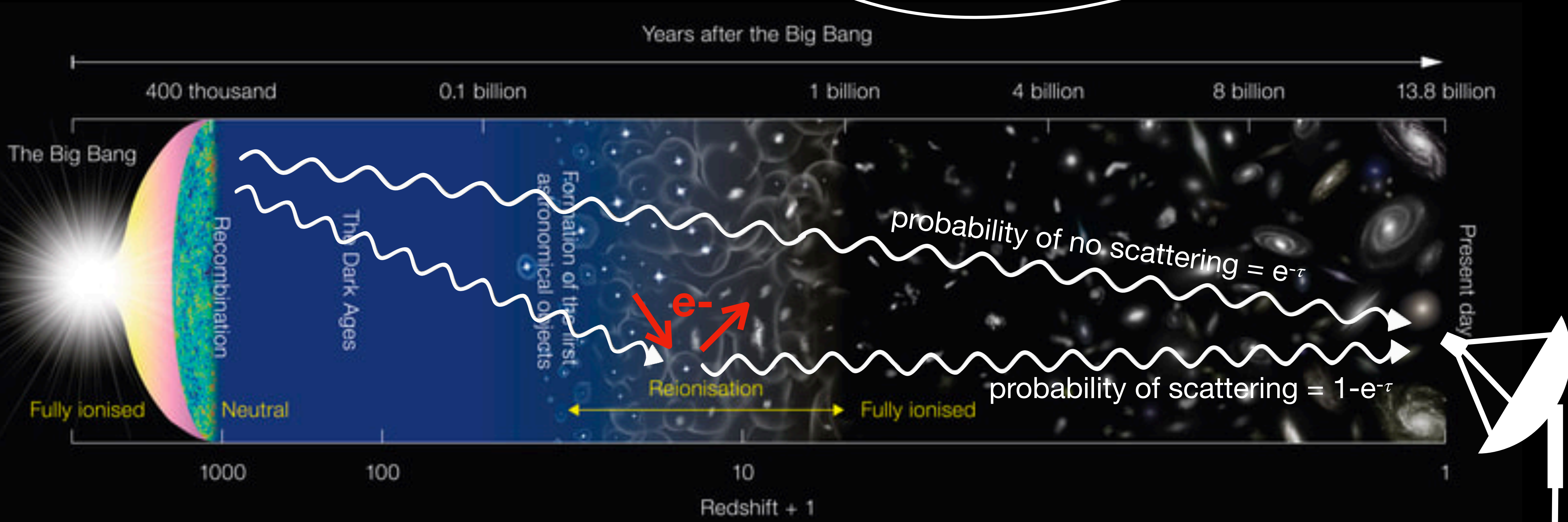

The rescattered photons have the temperature T̄ of the equilibrated ionized regions.

$$T_0 = \bar{T}_0 \left(1 + \Theta(\hat{\mathbf{n}})\right) e^{-\tau} + \bar{T}_0 \left(1 - e^{-\tau}\right) = \bar{T}_0 \left(1 + \Theta(\hat{\mathbf{n}}) e^{-\tau}\right)$$

observed anisotropies are suppressed by a factor $e^{-\tau}$

at the power spectrum level $C_\ell \rightarrow C_\ell e^{-2\tau}$

only on scales smaller than the horizon at reionization i.e. $\ell \gtrsim 10$

Josquin Errard, APC (CNRS)
Errard, Remazeilles et al. (ApJ, 2022)
CoPy, LPNHE, January 2023

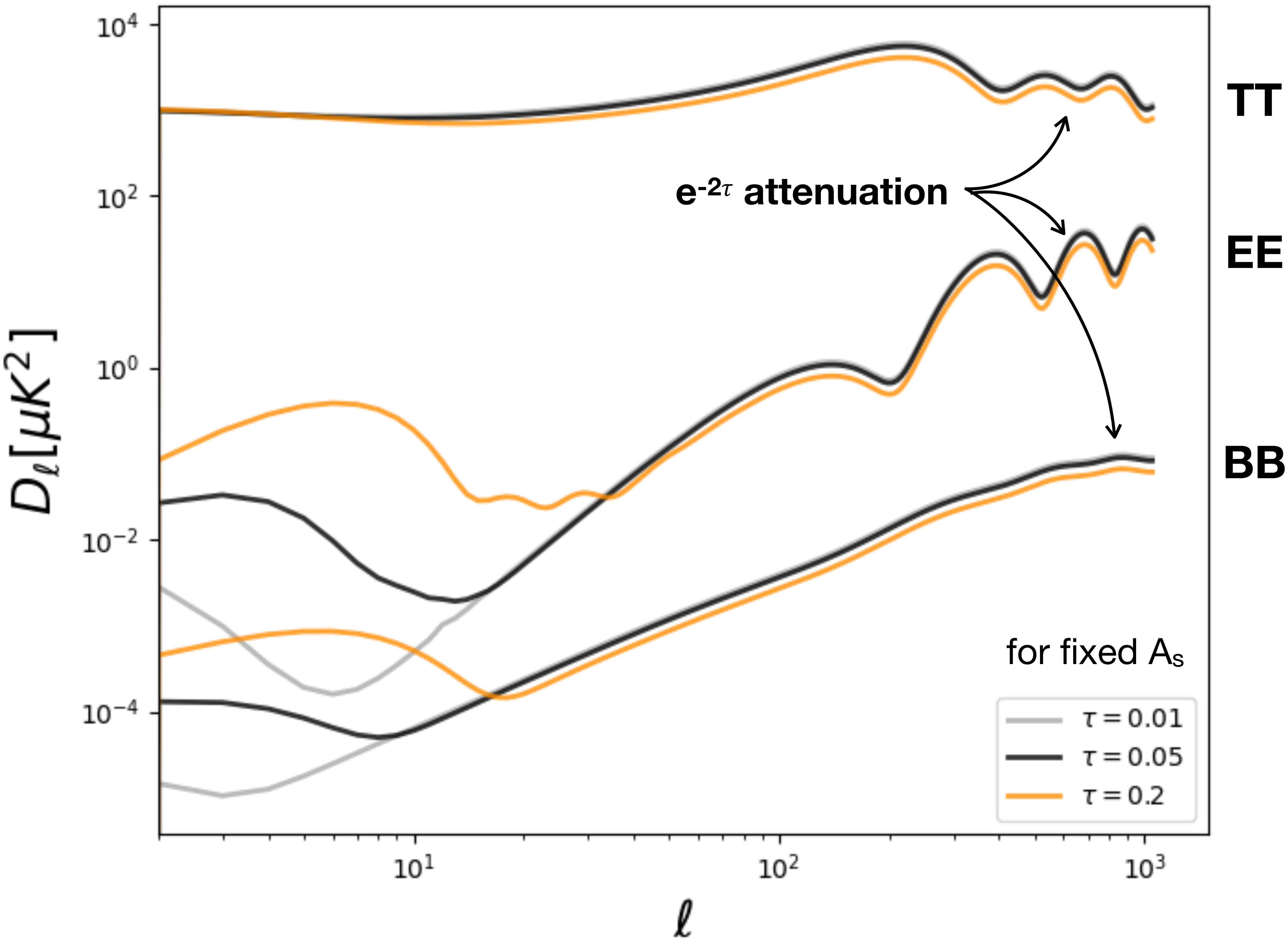

TT
EE
BB
e$^{-2\tau}$ attenuation
for fixed A_s
$\tau = 0.01$
$\tau = 0.05$
$\tau = 0.2$
$D_\ell [\mu K^2]$
ℓ
10^4
10^2
10^0
10^{-2}
10^{-4}
10^1
10^2
10^3

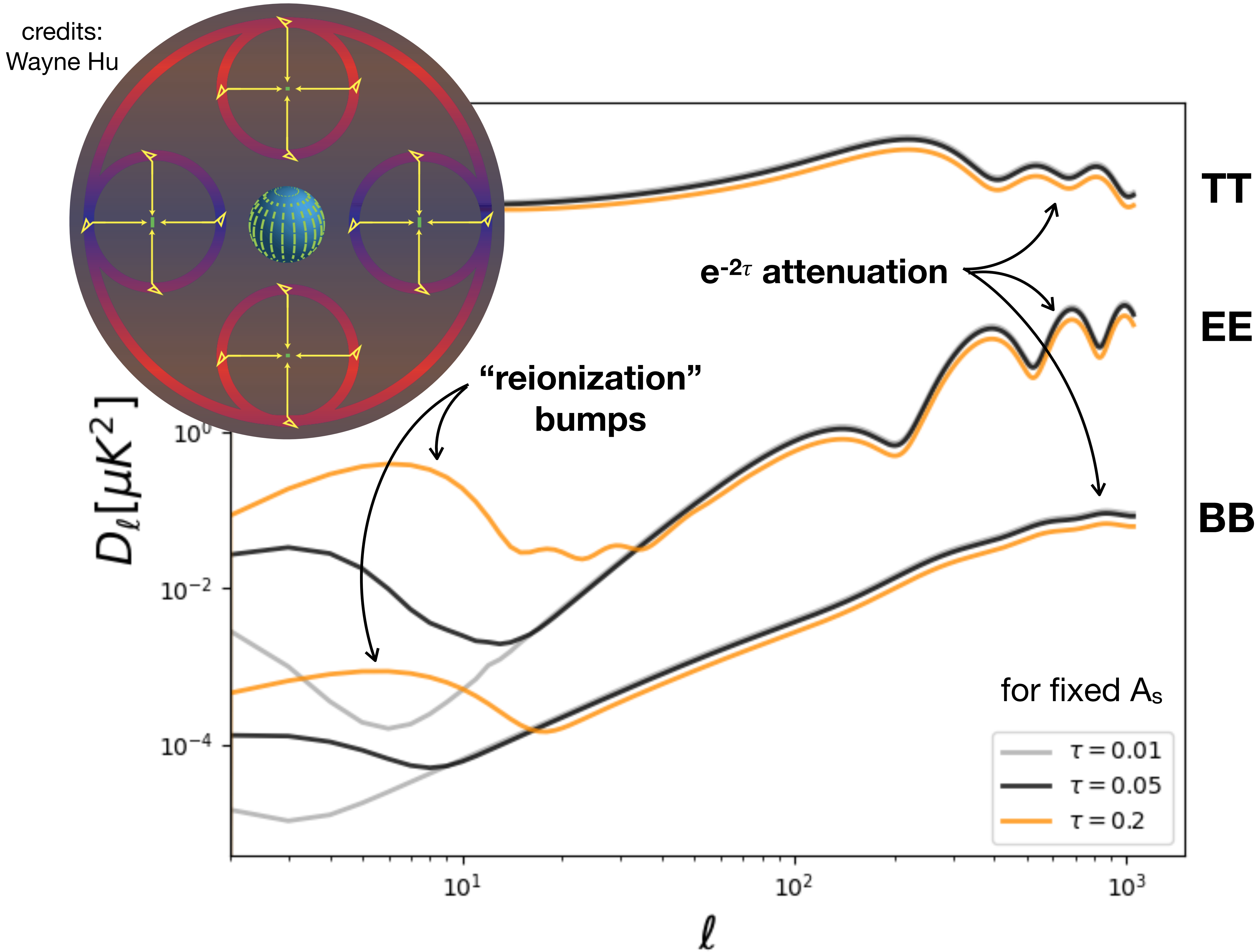

credits:
Wayne Hu
TT
EE
BB
e-2τ attenuation
“reionization” bumps
for fixed As
τ = 0.01
τ = 0.05
τ = 0.2
$D_\ell[\mu K^2]$
ℓ
10^0
10^{-2}
10^{-4}
10^1
10^2
10^3

credits:
Wayne Hu

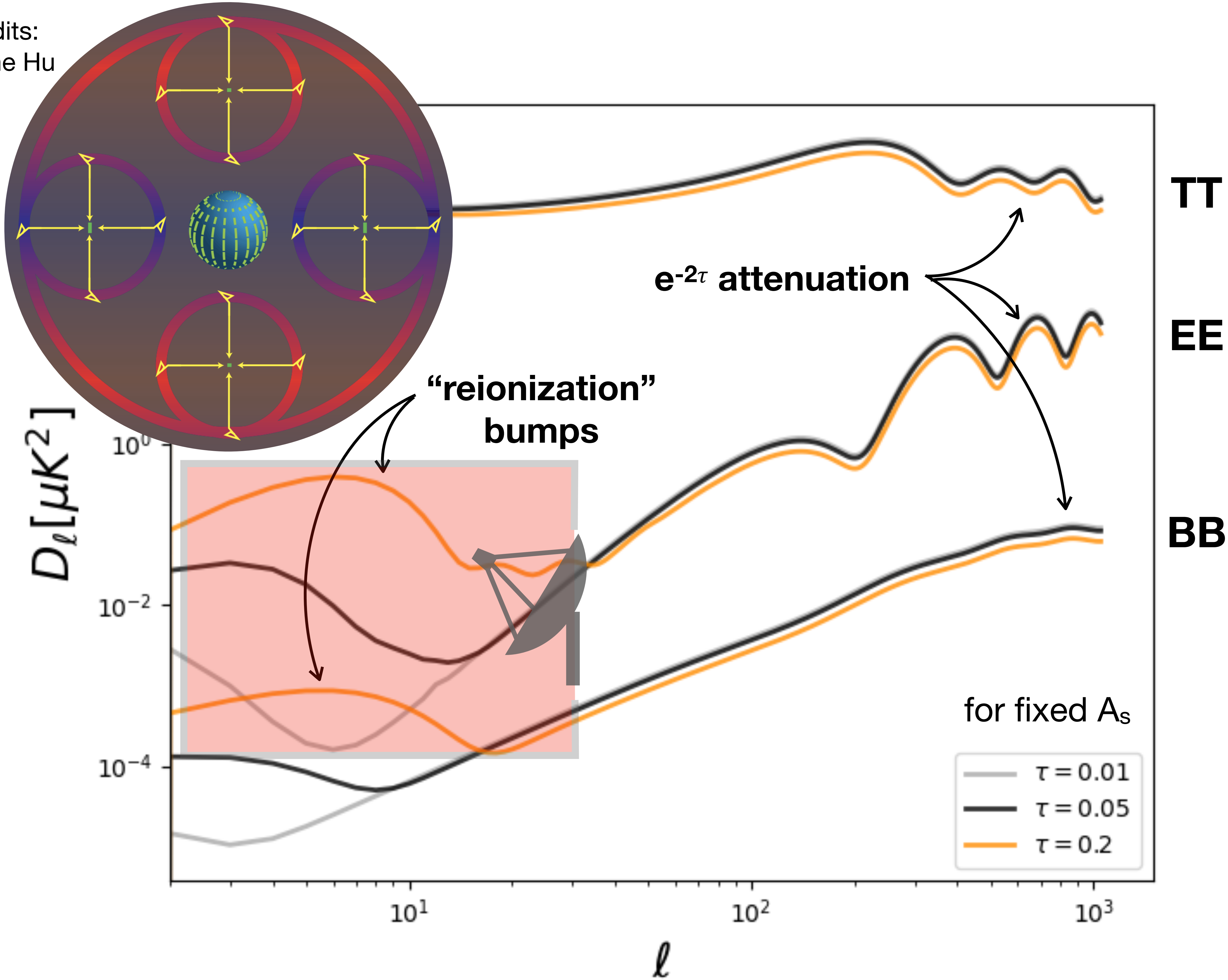

Projected 1σ and 2σ constraints on the mean redshift (z_{re}) and duration of reionization (Δz_{re})

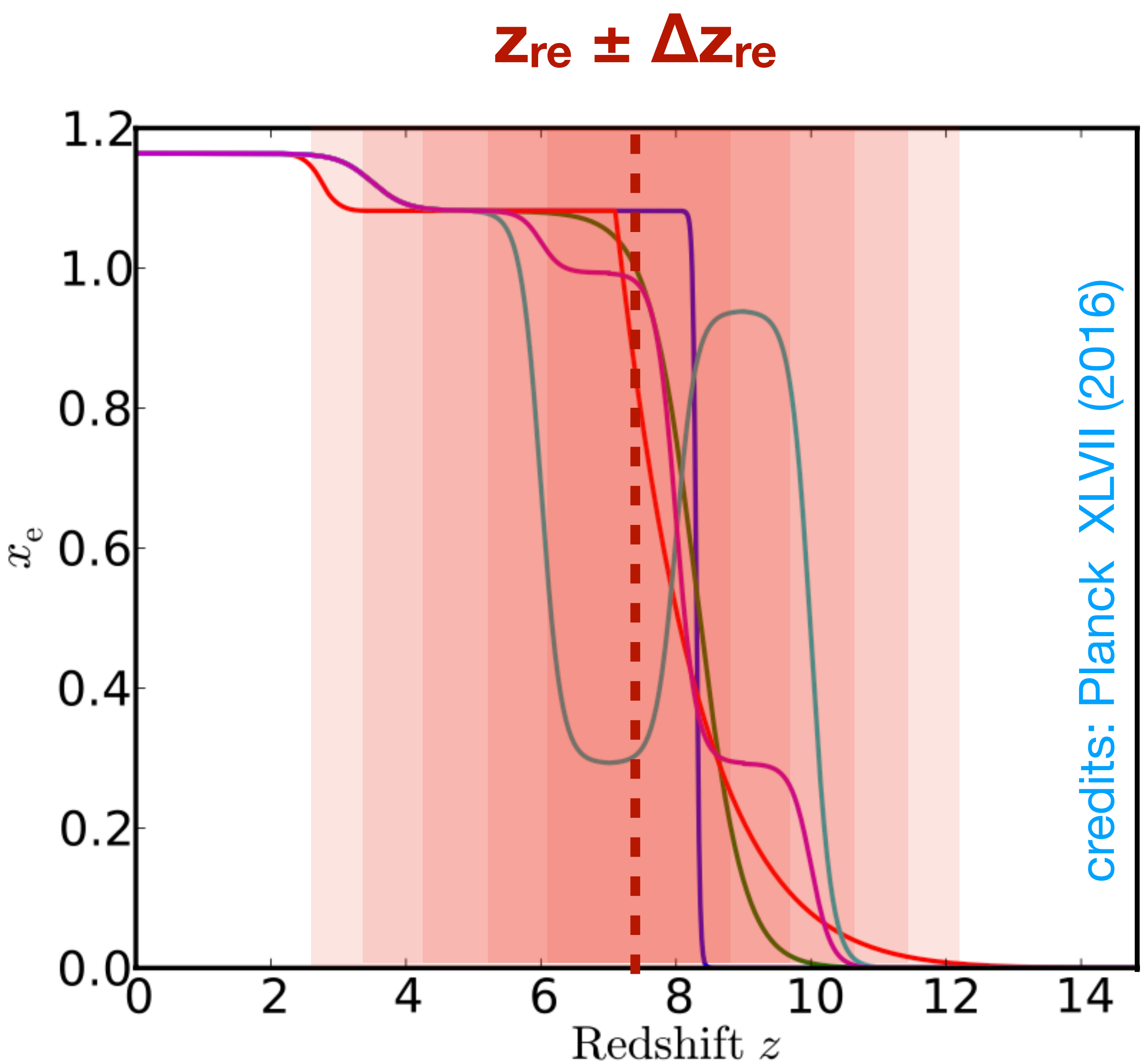

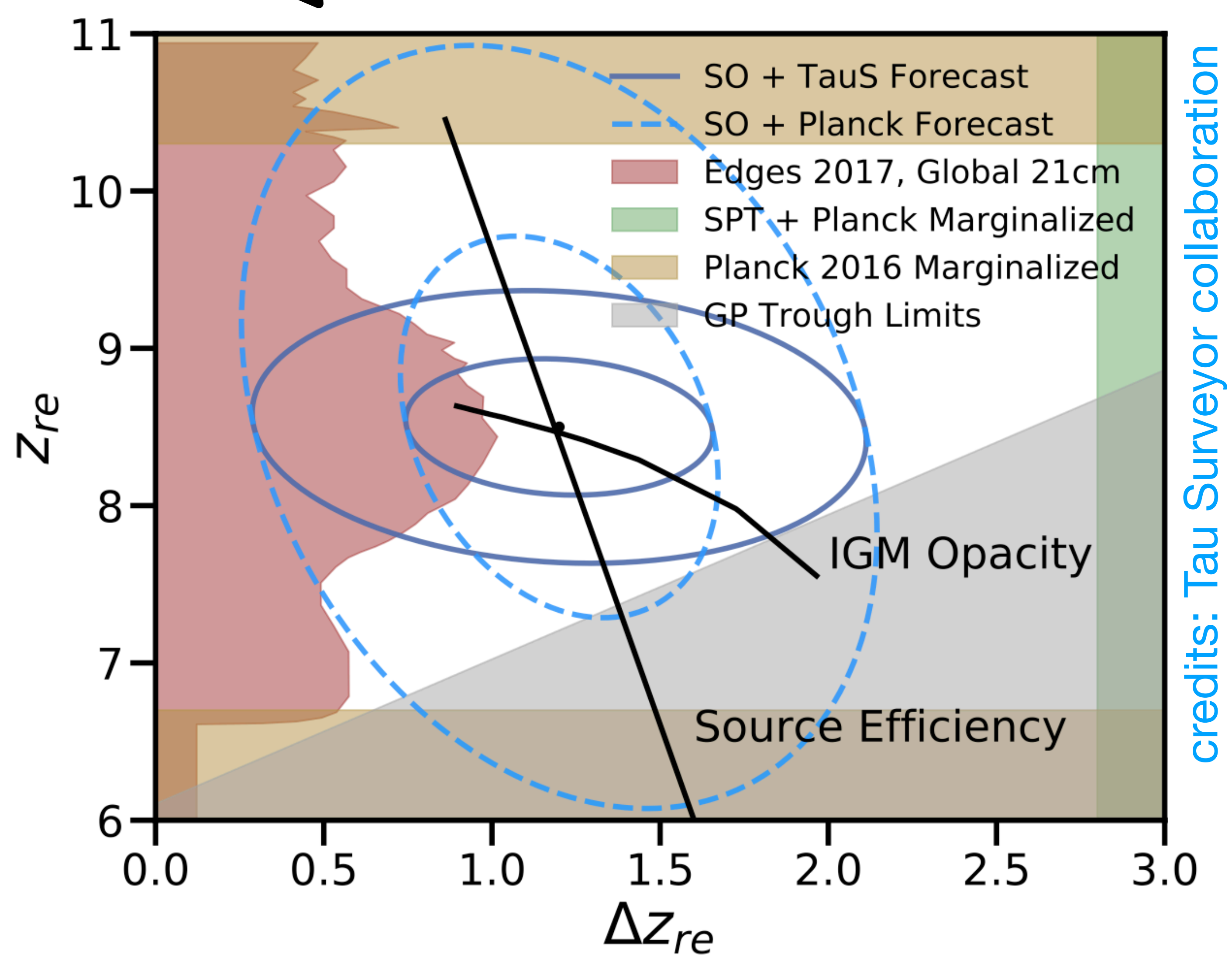

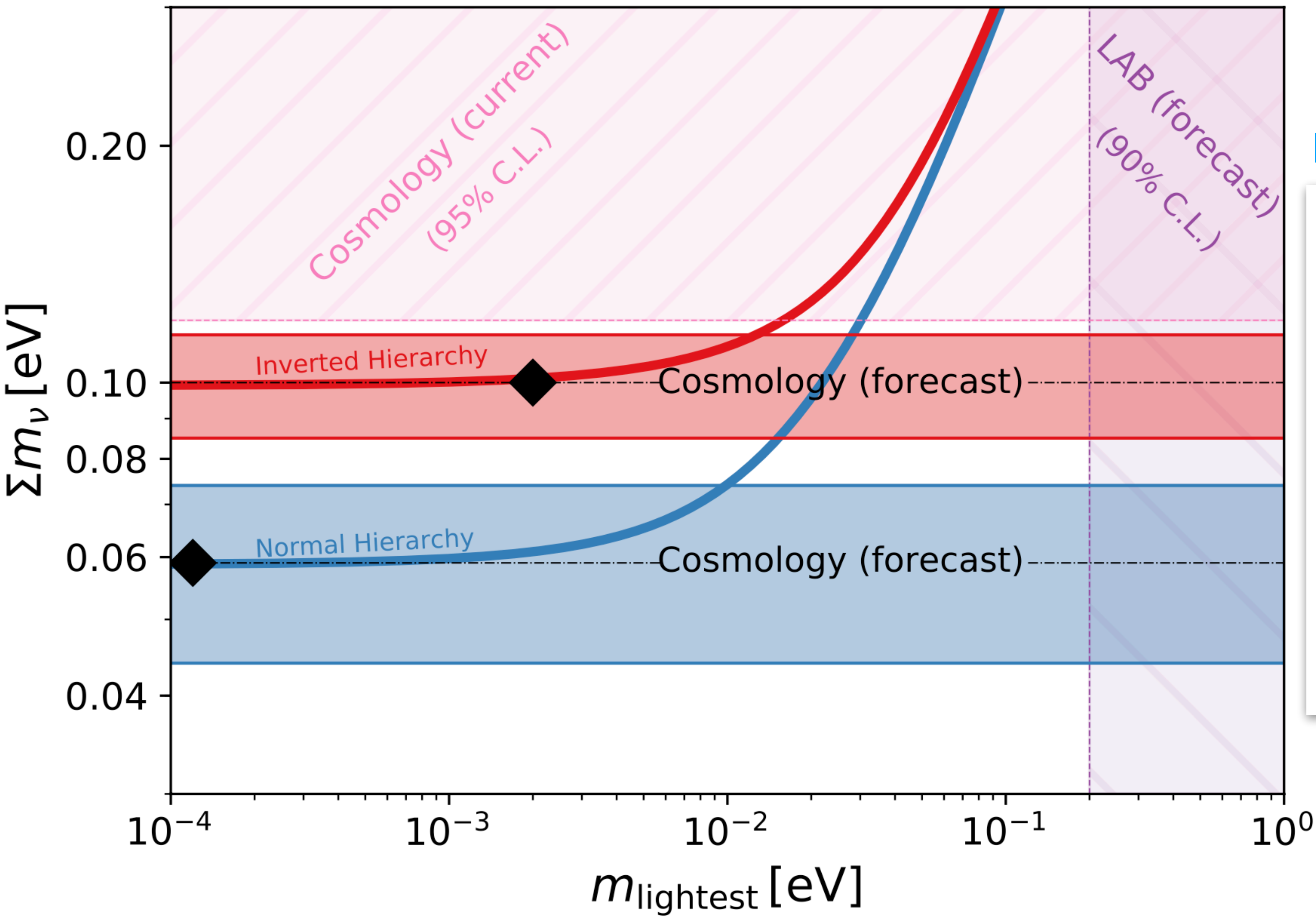

Dvorkin et al. (2019)

Precision measurements of τ are also the only way

- to break crucial degeneracies between cosmological parameters
- provide the tightest constraint foreseeable in the near future on the neutrino mass

CMB-S4 Collaboration (2016)

non-zero masses of neutrinos hint at the existence of additional degrees of freedom beyond the Standard Model

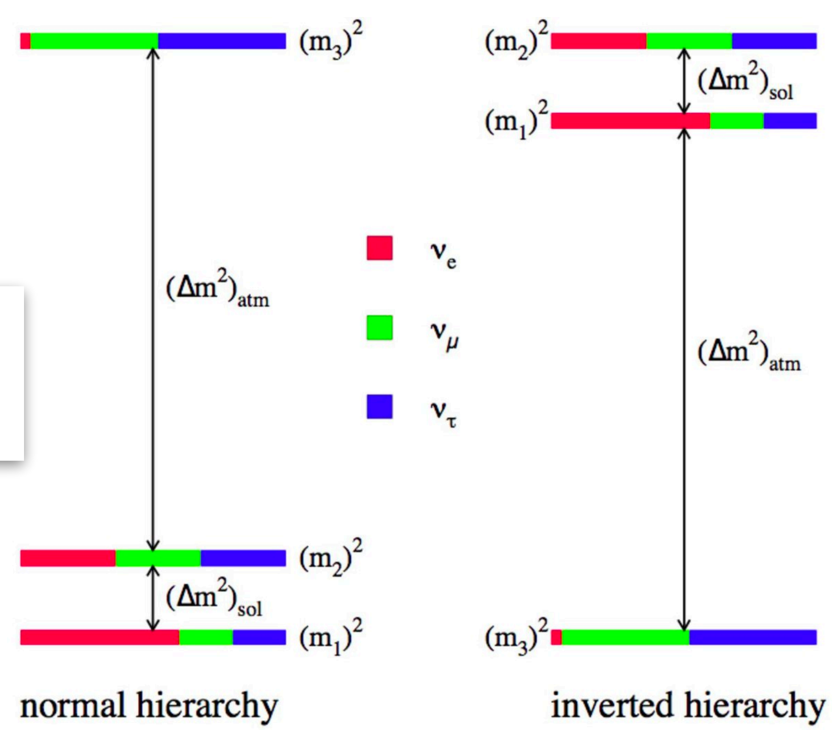

Challenges related to measuring τ through CMB observations

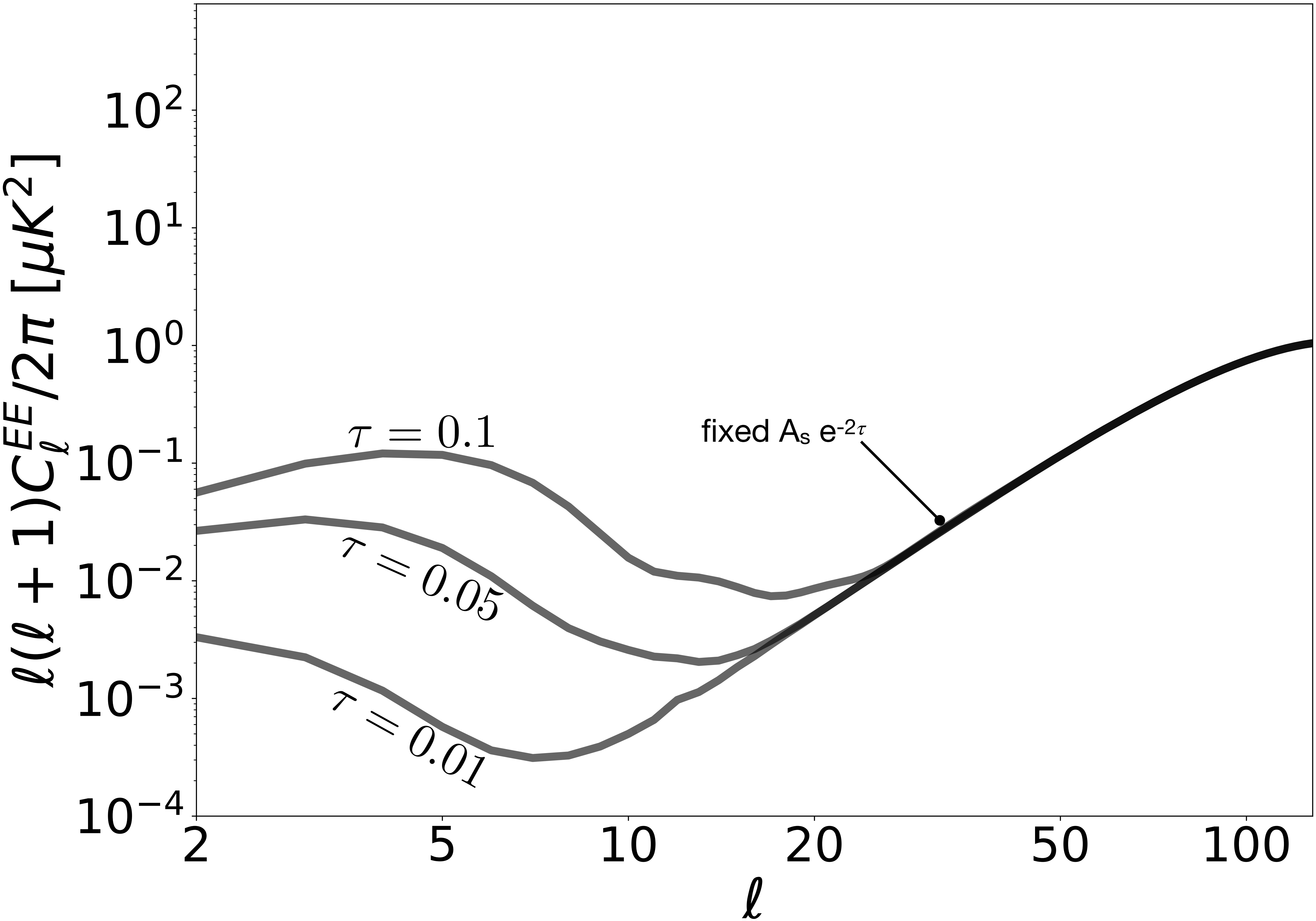

Challenges related to measuring τ through CMB observations

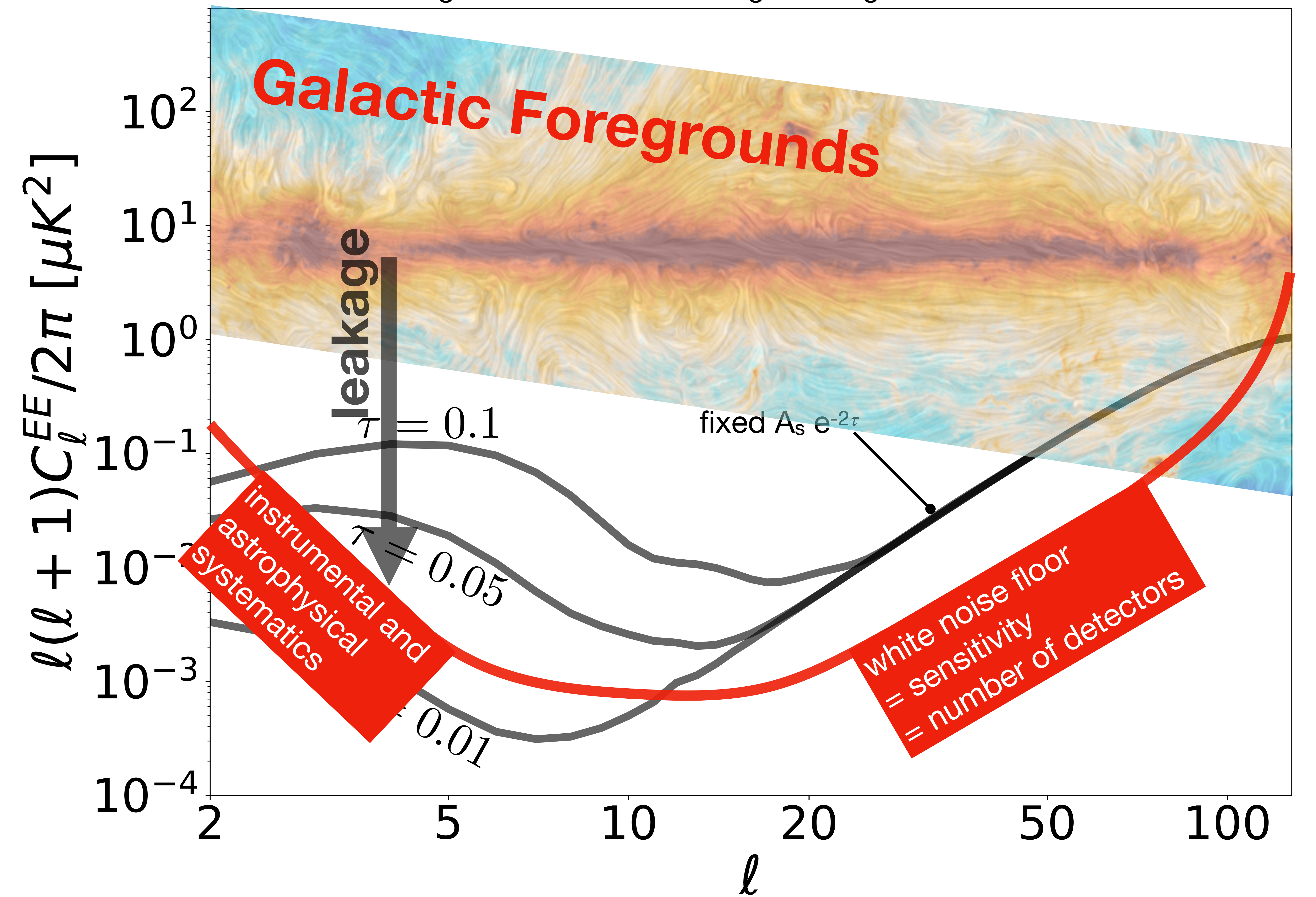

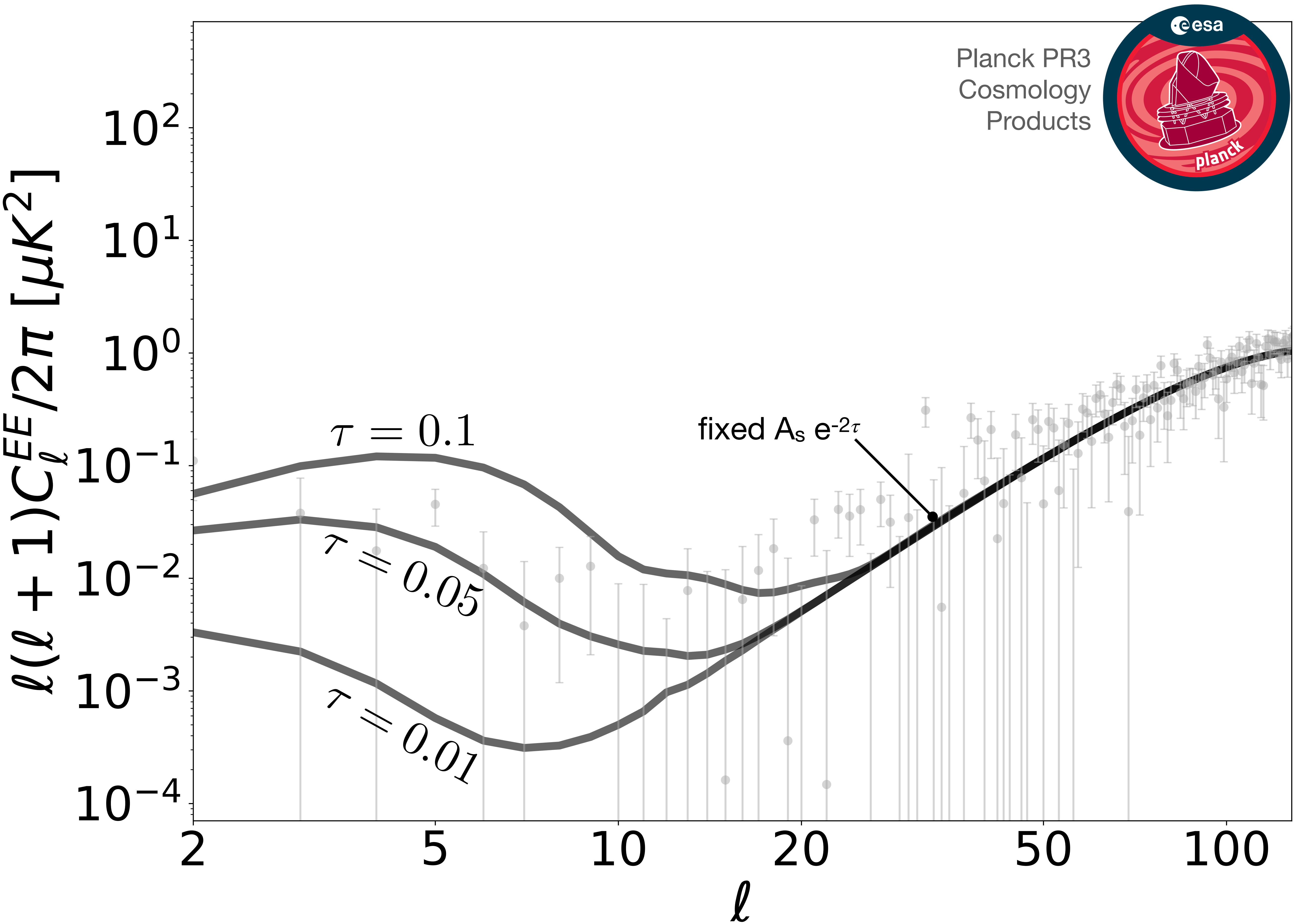

Planck PR3
Cosmology
Products
esa
planck
$\ell(\ell+1)C_\ell^{EE}/2\pi\ [\mu K^2]$
10^2
10^1
10^0
10^{-1}
10^{-2}
10^{-3}
10^{-4}
$\tau = 0.1$
$\tau = 0.05$
$\tau = 0.01$
fixed $A_s\ e^{-2\tau}$
2
5
10
20
50
100
ℓ

$$\tau = 0.054 \pm 0.007$$ Planck collaboration (2020)

$$\longrightarrow \sigma(\tau) = 0.006$$ Pagano et al. (2020)

These measurements have revolutionized our understanding of the reionization epoch [Planck XLVII], and, in combination with large-scale structure data, gave the tightest constraint yet on the neutrino mass [Planck VI]

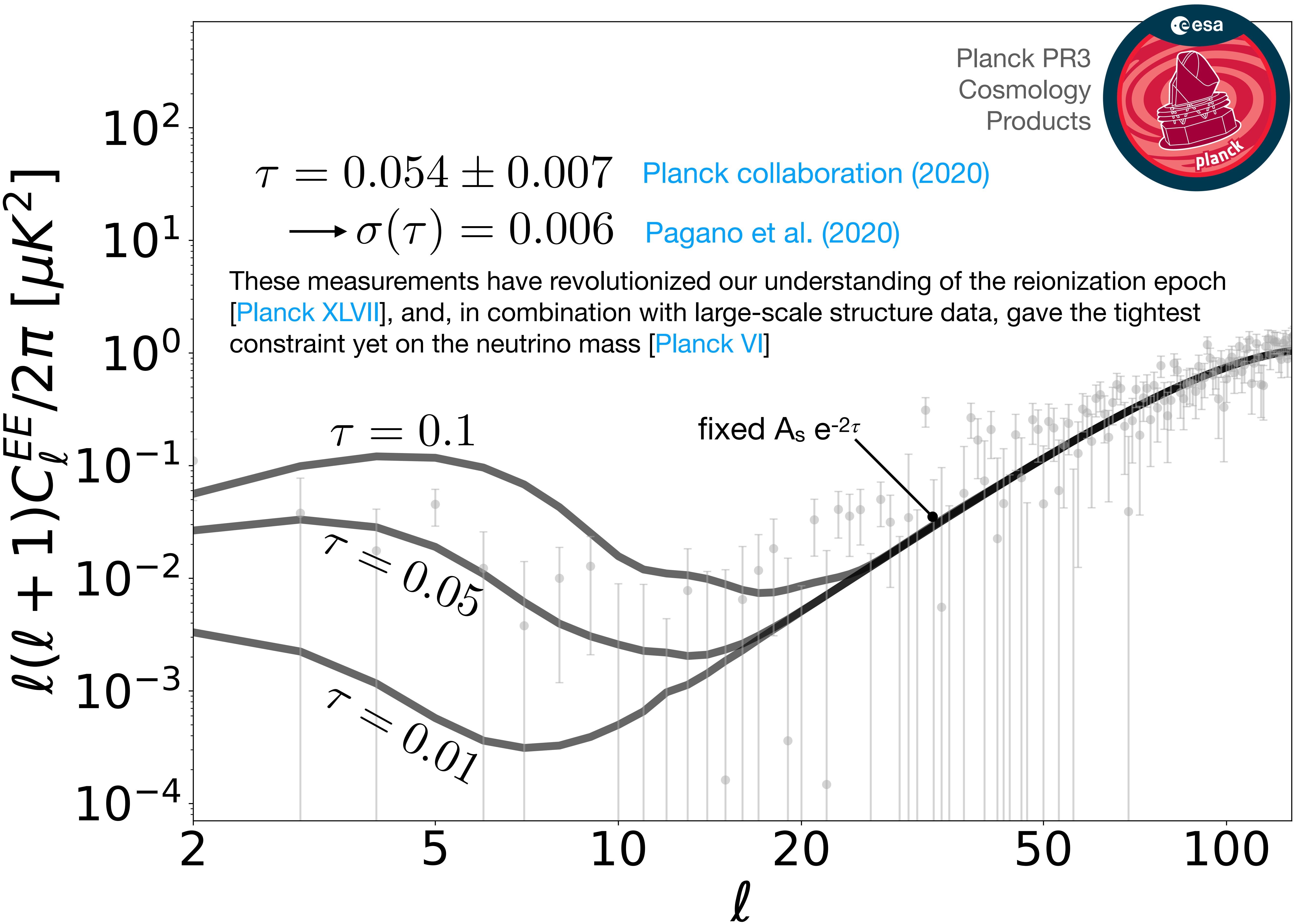

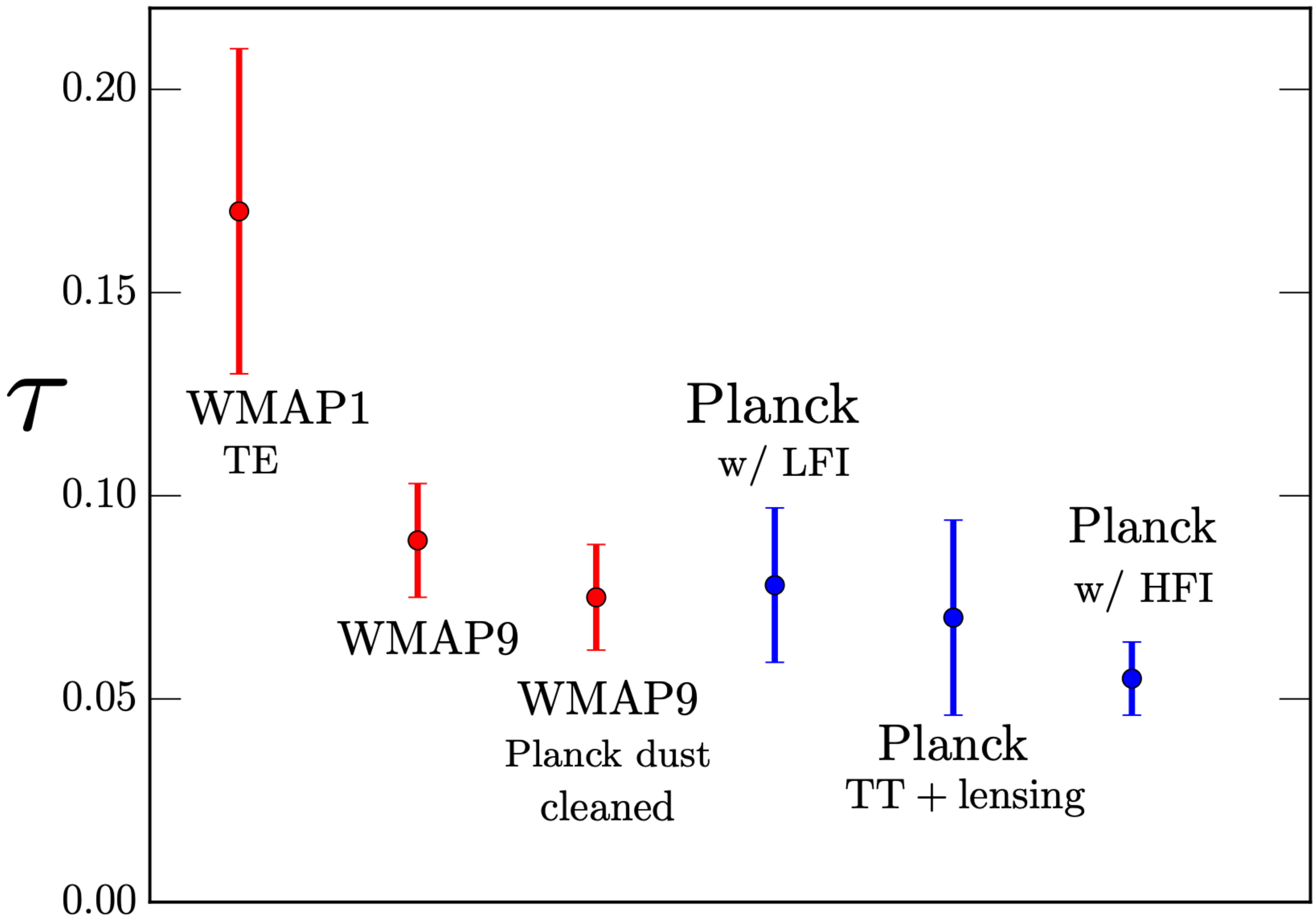

credits: Heinrich, Miranda & Hu arXiv:1609.04788

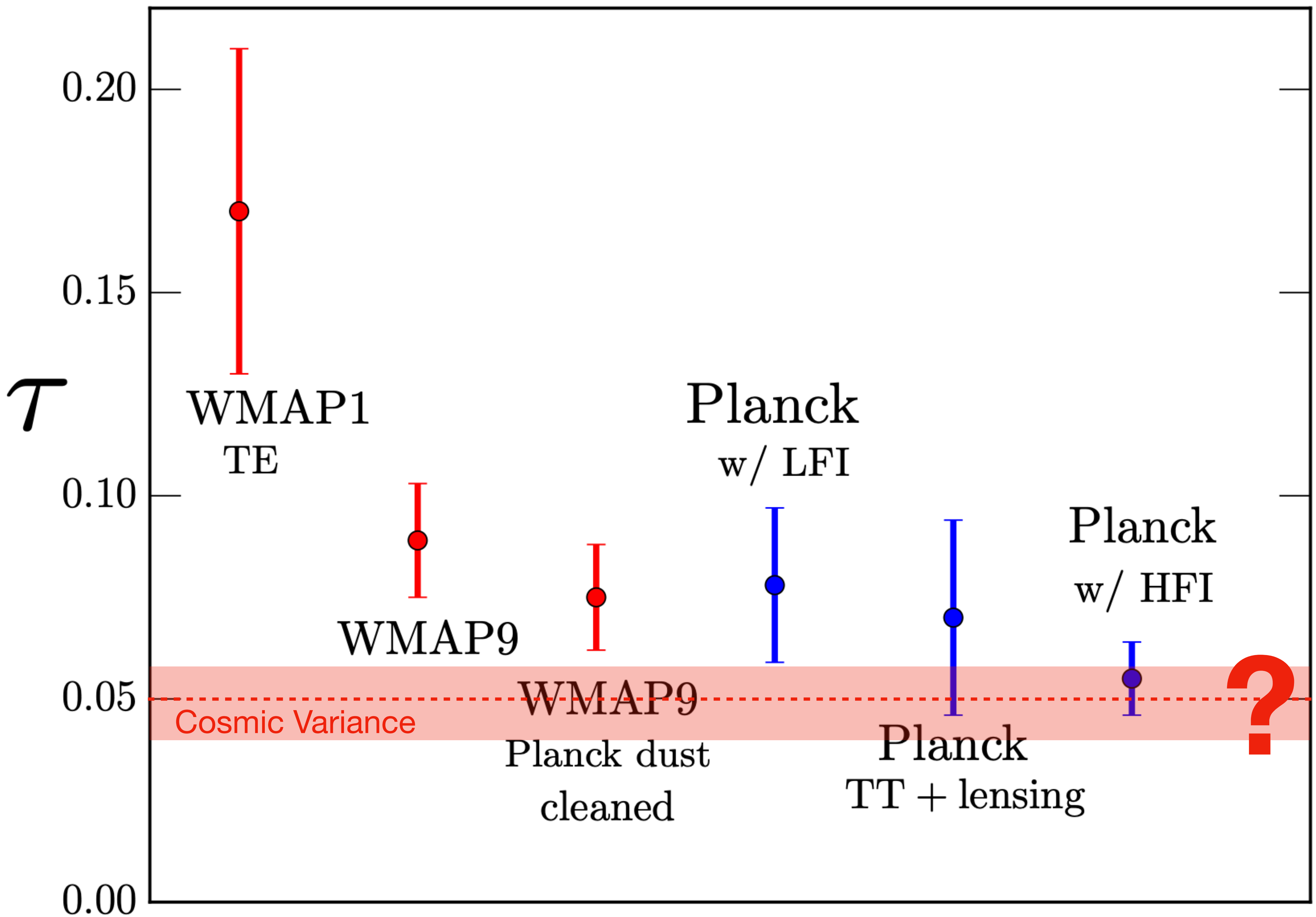

credits: Heinrich, Miranda & Hu arXiv:1609.04788

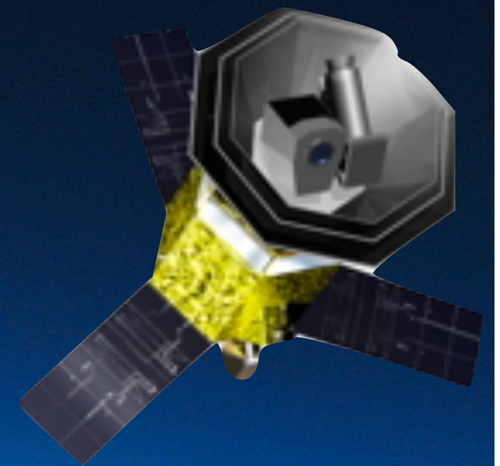

space

- relatively high cost
- great environment
- large fraction of the sky, no frequency limitation

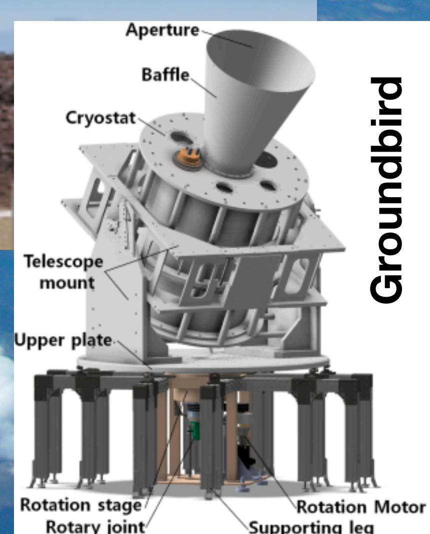

ground

- relatively low-medium cost
- high difficulties to constrain large angular scales due to the environment
- limited frequency bands due to atmosphere

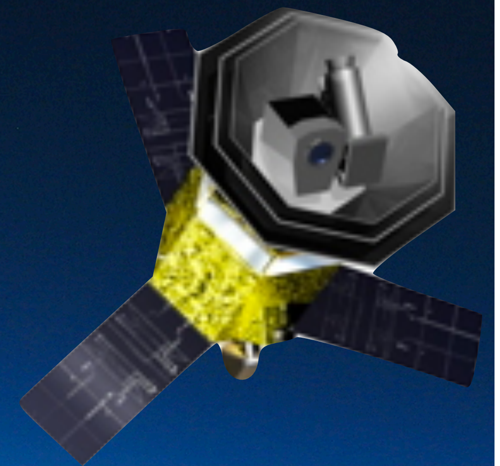

space
- relatively high cost
- great environment
- large fraction of the sky, no frequency limitation

Tau-Surveyor

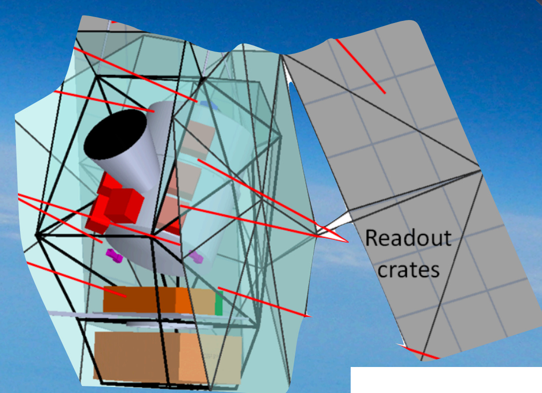

Taurus

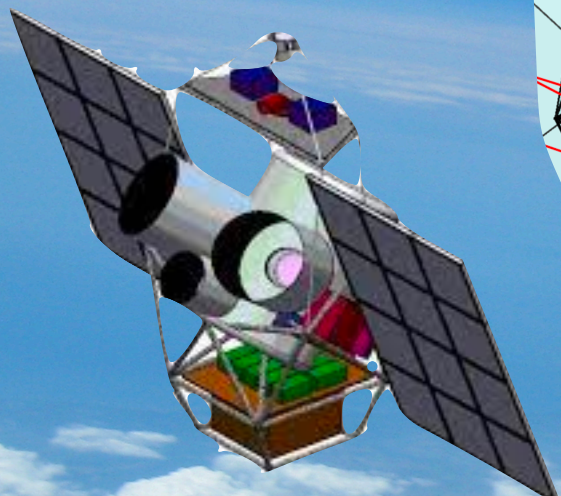

balloon
- risky, but relatively low cost
- atmospheric contamination greatly reduced
- >50% sky fraction, high frequency doable

CLASS

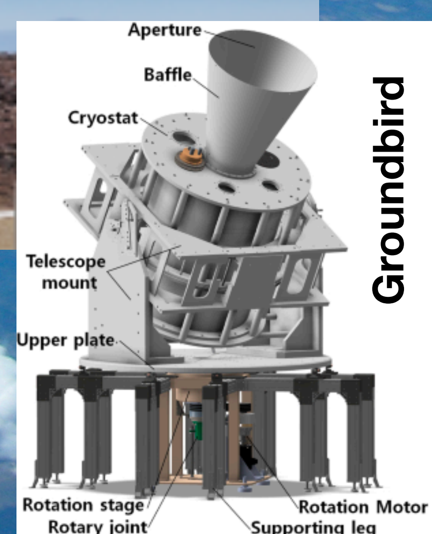

ground
- relatively low-medium cost
- high difficulties to constrain large angular scales due to the environment
- limited frequency bands due to atmosphere

Constraints on the Optical Depth to Reionization from Balloon-borne Cosmic Microwave Background Measurements

Josquin Errard[1], Mathieu Remazeilles[2,3], Jonathan Aumont[4], Jacques Delabrouille[5], Daniel Green[6], Shaul Hanany[7], Brandon S. Hensley[8], and Alan Kogut[9]

➔ How well can a **CMB balloon** perform in measuring the reionization optical depth?

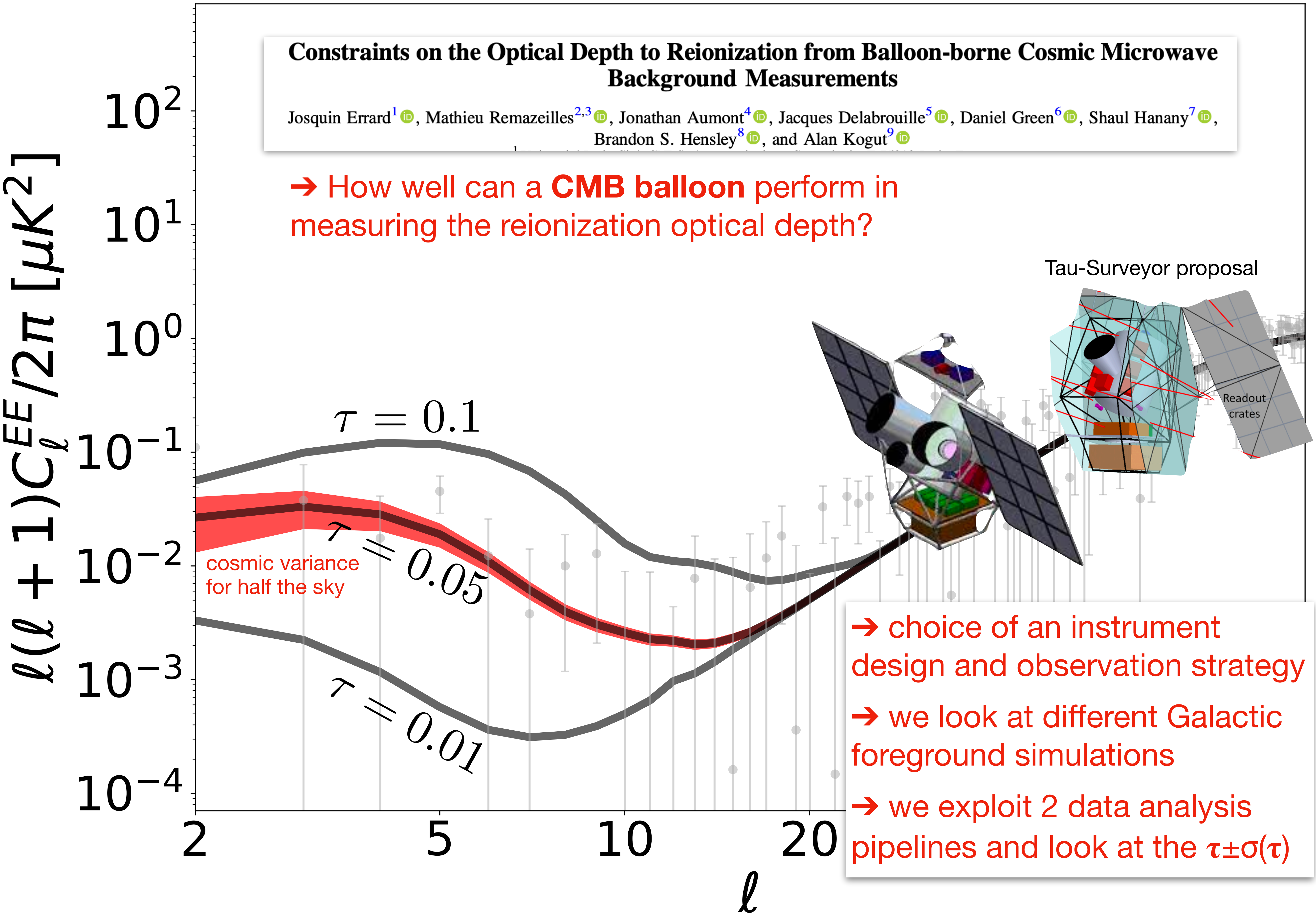

➔ choice of an instrument design and observation strategy

➔ we look at different Galactic foreground simulations

➔ we exploit 2 data analysis pipelines and look at the $\tau \pm \sigma(\tau)$

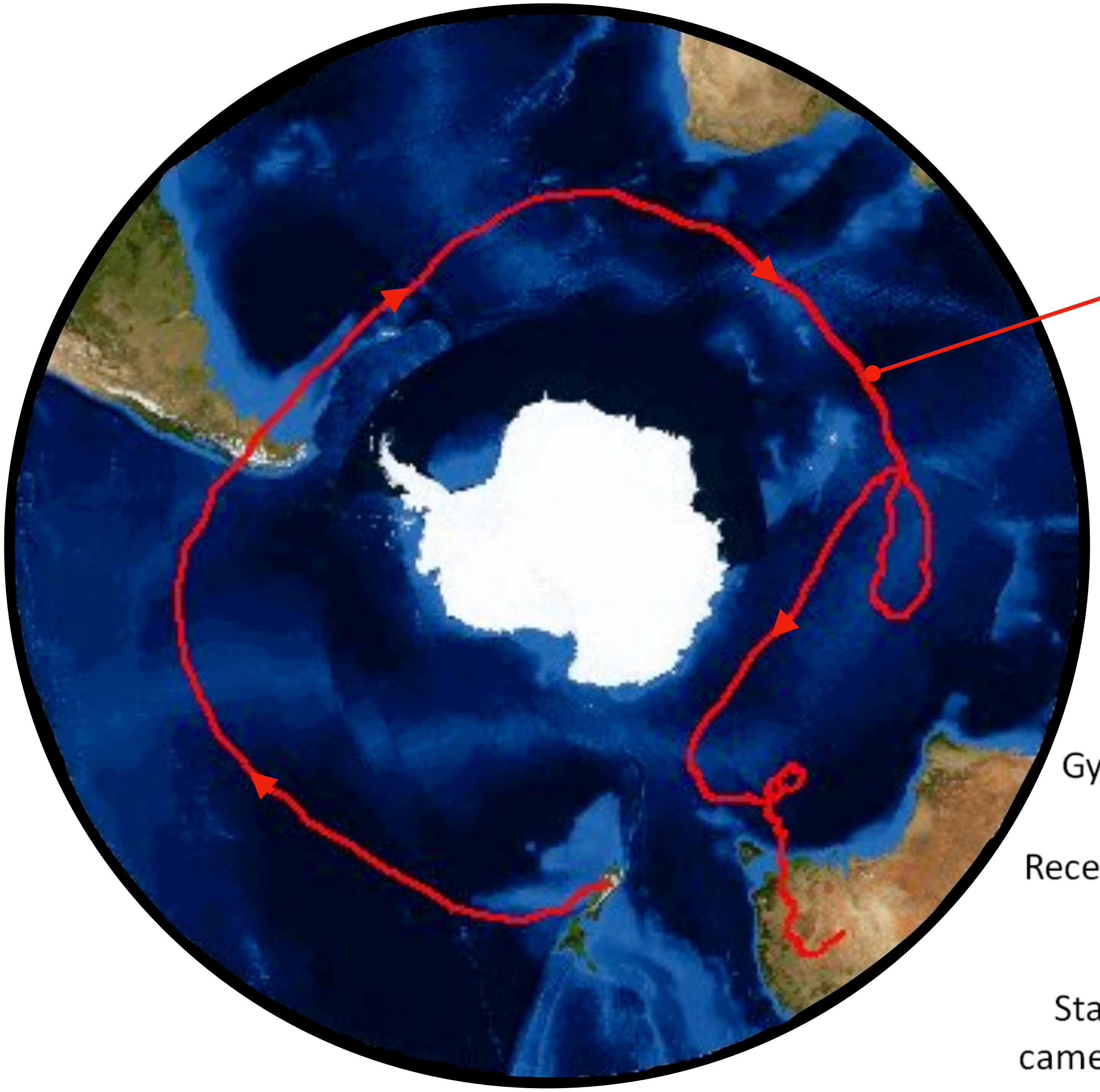

ultralong-duration flight from Wanaka, New Zealand.
(40 nights assumed)

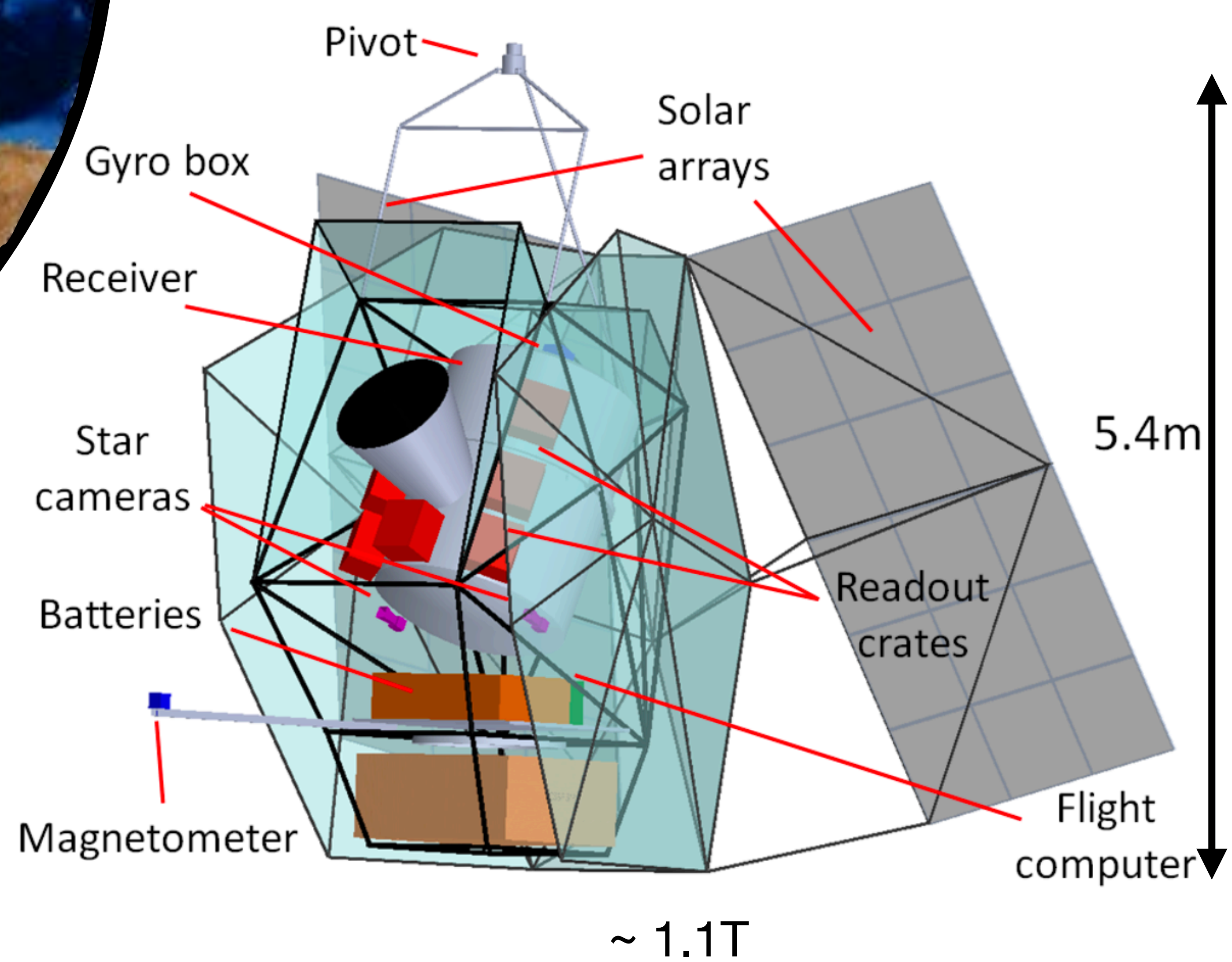

57% of the sky can be observed using night-time only

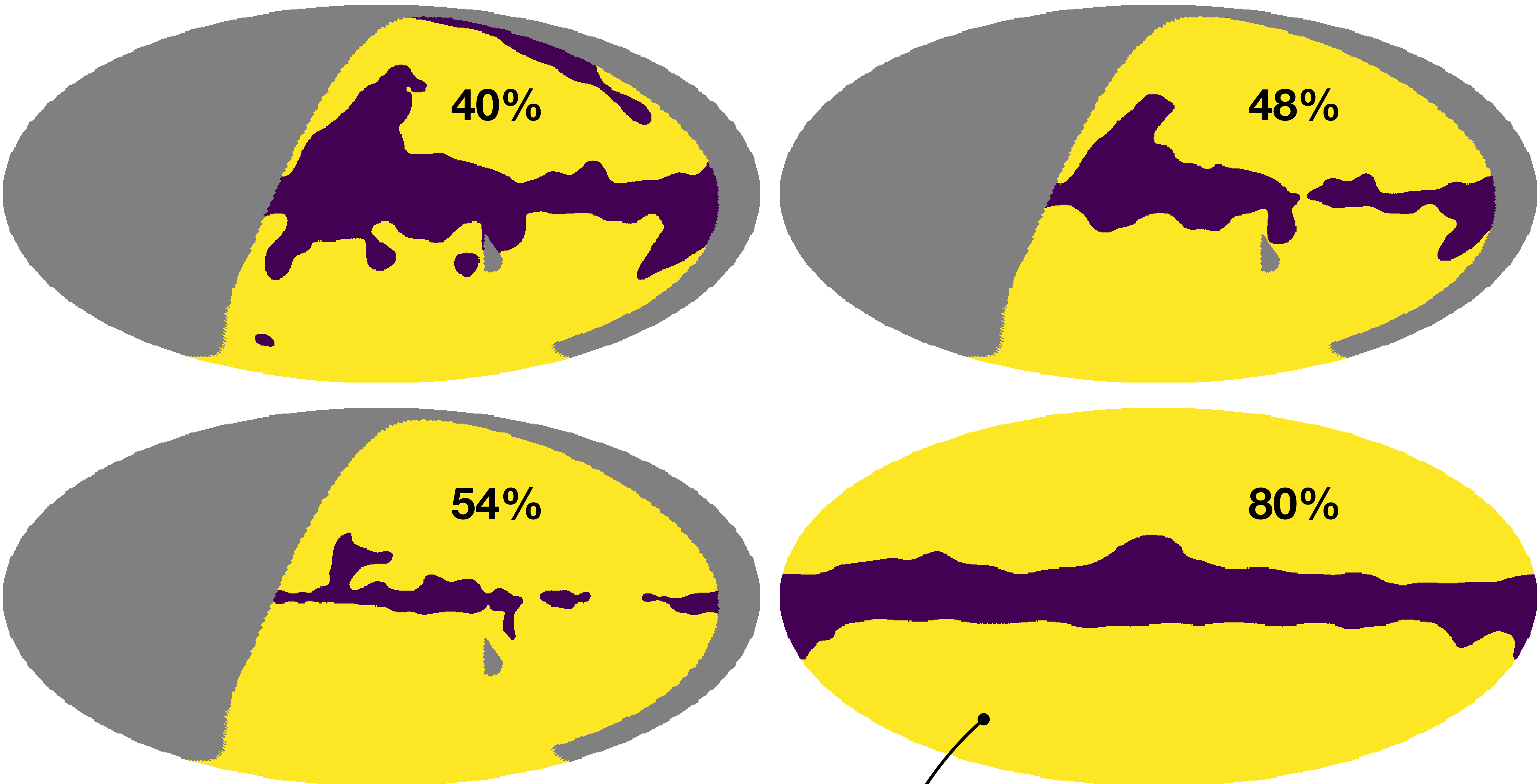

achievable with 2 balloons, one in the North and one in the South!

Josquin Errard, APC (CNRS)
Errard, Remazeilles et al. (ApJ, 2022)
CoPy, LPNHE, January 2023

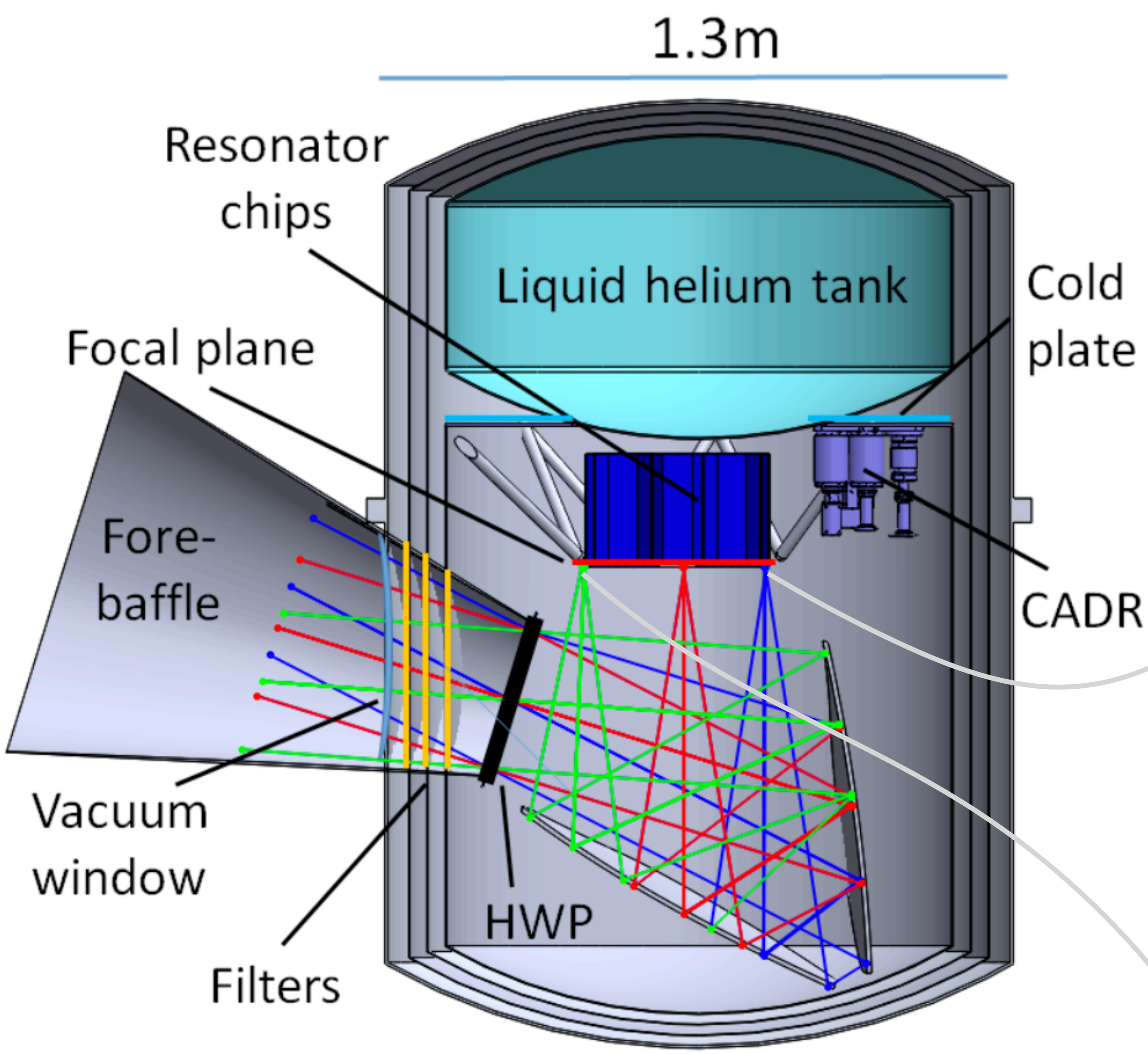

- 6 frequency bands
- 15k detectors
- 7 uK-arcmin sensitivity in polarization
- beam 14-35arcmin

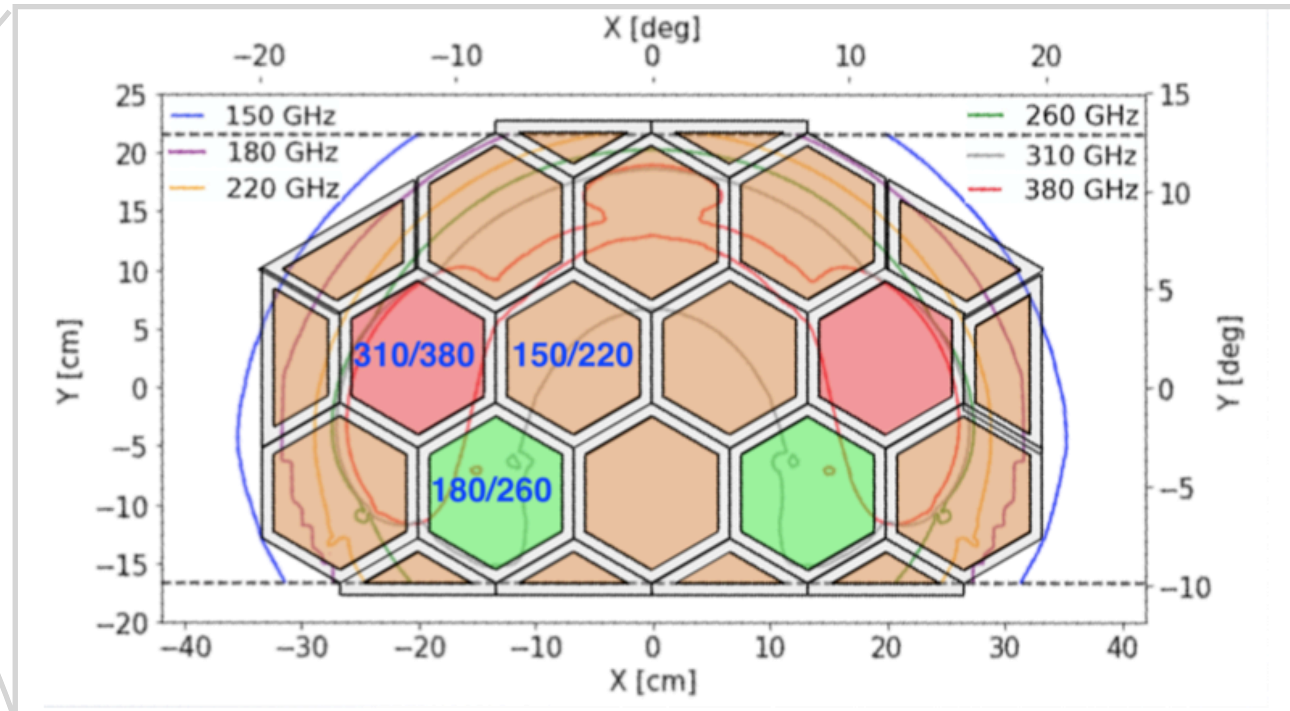

Pixel Type	Frequency Band (GHz)	Beam Size (arcmin)	Detector NET[a] (μK $\sqrt{s}$)	Number of Detectors	Array NET[a] (μK $\sqrt{s}$)	Polarization Weight (μK arcmin)
Low	150	35	64	4410	0.96	9.5
Frequency	220	24	87	3234	1.5	15
Middle	180	29	90	1800/3000	2.1/1.65	21/16
Frequency	260	20	141	1800/3000	3.3/2.6	33/25.5
High	310	17	350	2028/0	7.8/0	77/0
Frequency	380	14	833	2028/0	18.5/0	183/0
Total			42	15,300/13,644	0.74/0.70	7.3/6.9

Challenges: focus on dust domination

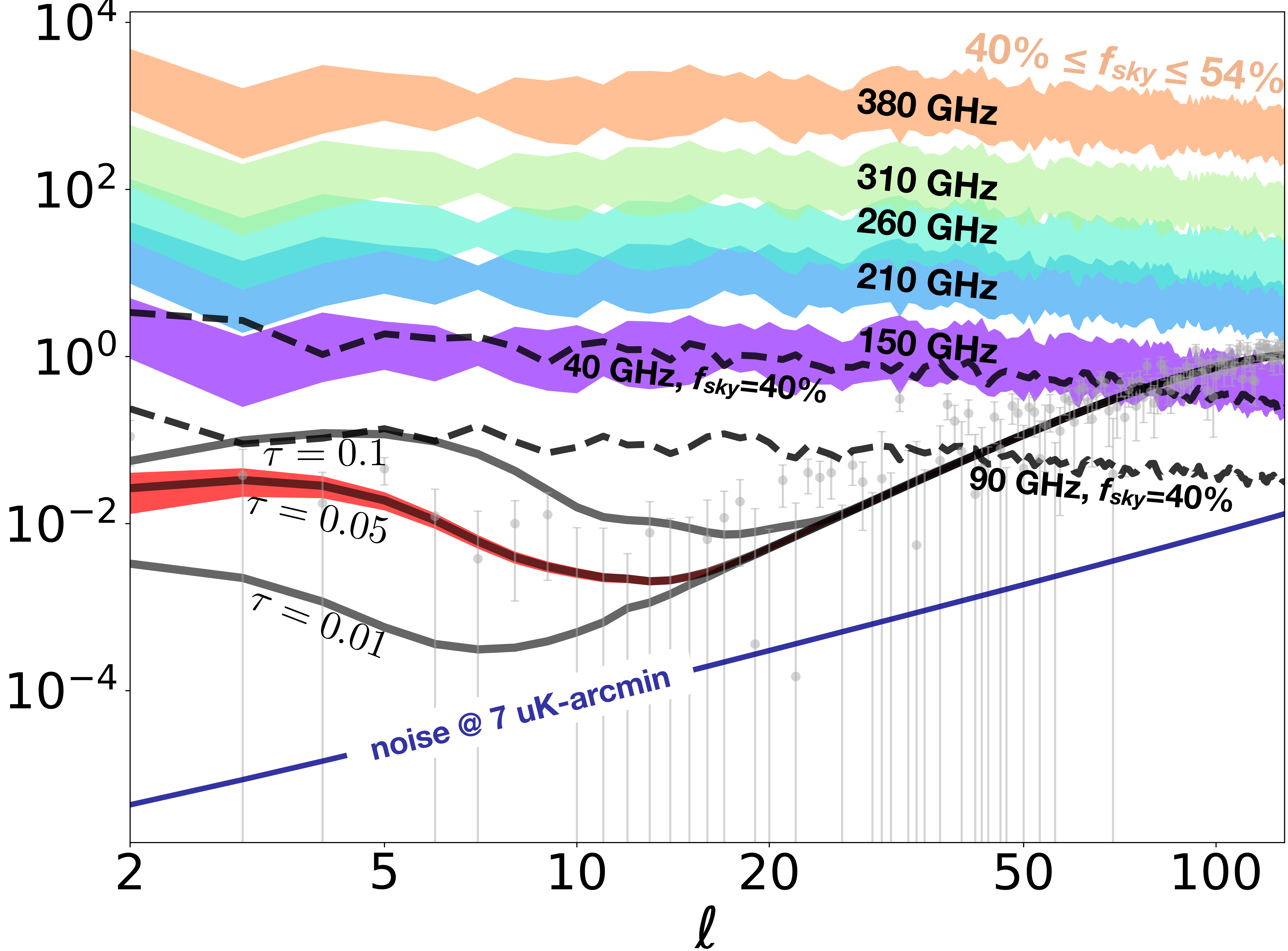

Challenges: focus on dust domination

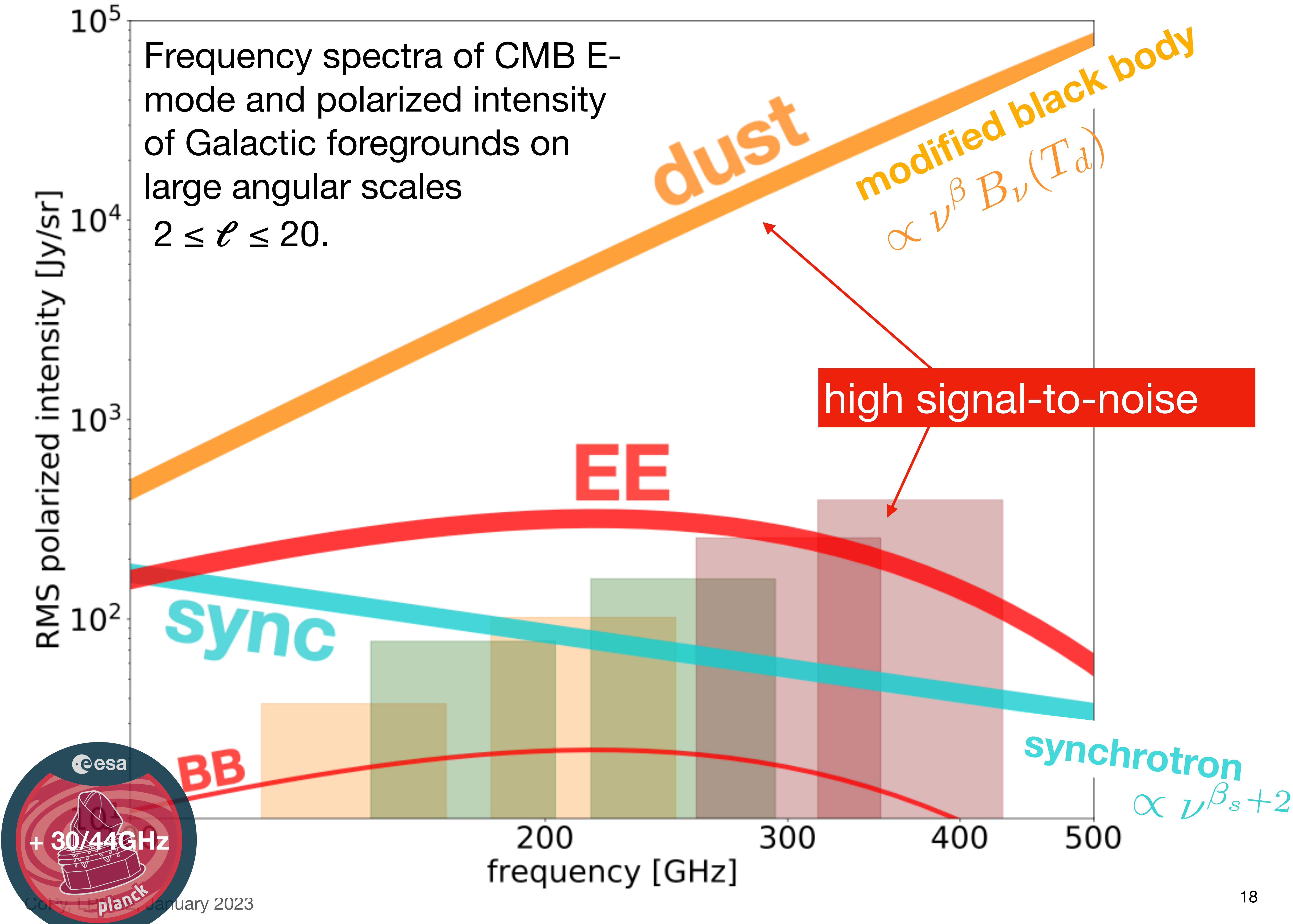

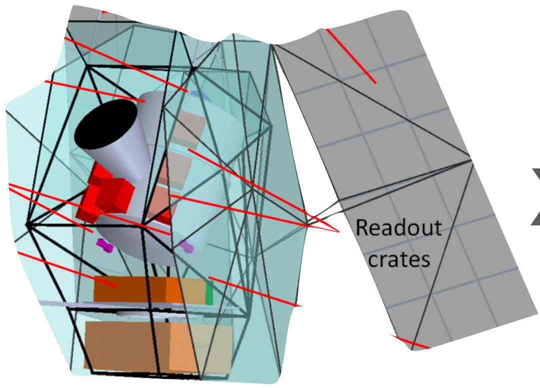

x

sky simulations

CMB + noise + galactic foregrounds

x 10

d1s1

d7s3

MKD

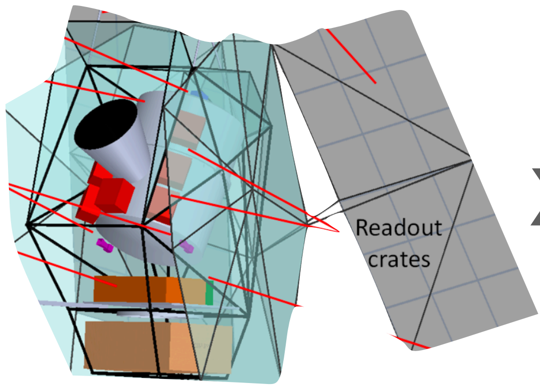

X

sky simulations

CMB + noise + galactic foregrounds

x 10

d1s1 d7s3 MKD

Zonca et al. 2021

$$Q^{\mathrm{d1}}_{\nu,p} = A^{Q}_{d,p}\left(\frac{\nu}{\nu_0}\right)^{\beta_{d,p}} B_\nu(T_{d,p})$$

$$Q^{\mathrm{s1}}_{\nu,p} = A^{Q}_{s,p}\left(\frac{\nu}{\nu_0}\right)^{\beta_{s,p}+2}$$

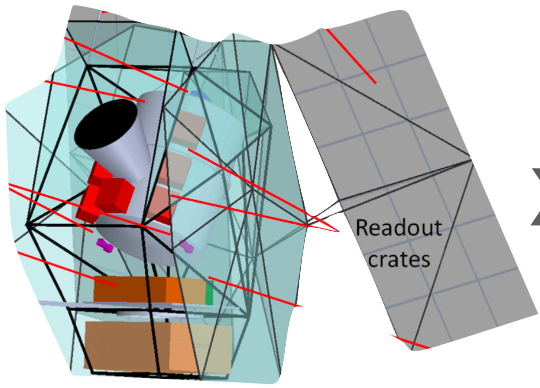

X

sky simulations

CMB + noise + galactic foregrounds

x 10

d1s1 d7s3 MKD

Zonca et al. 2021

$$Q^{\mathrm{d1}}_{\nu,p} = A^{Q}_{d,p}\left(\frac{\nu}{\nu_0}\right)^{\beta_{d,p}} B_\nu(T_{d,p})$$

$$Q^{\mathrm{s1}}_{\nu,p} = A^{Q}_{s,p}\left(\frac{\nu}{\nu_0}\right)^{\beta_{s,p}+2}$$

Draine & Hensley 2013

$$\log_{10}\mathcal{U}_p = (4 + \beta_{d,p})\log_{10}\left(\frac{T_{d,p}}{\langle T_d\rangle}\right)$$

$$Q^{\mathrm{d7}}_{\nu,p} = A^{Q}_{d,p}\,\frac{f_\nu(\mathcal{U}_p)}{f_{\nu_0}(\mathcal{U}_p)}$$

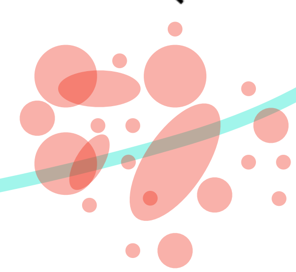

“ […] the dust emission is modeled as arising from a population of dust grains with different compositions, sizes, and temperatures, as described by Hensley (2015).”

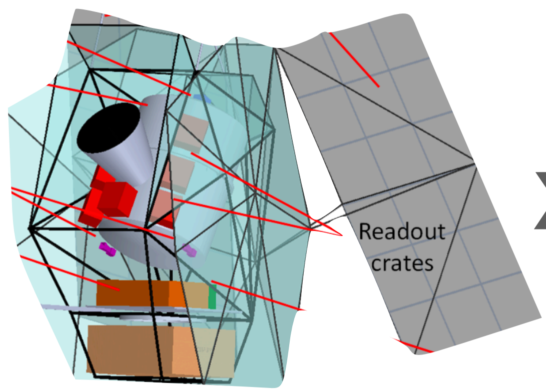

X

sky simulations

CMB + noise + galactic foregrounds

x 10

d1s1 d7s3 MKD

Zonca et al. 2021

$$Q^{\mathrm{d1}}_{\nu,p} = A^{Q}_{d,p}\left(\frac{\nu}{\nu_0}\right)^{\beta_{d,p}} B_\nu(T_{d,p})$$

$$Q^{\mathrm{s1}}_{\nu,p} = A^{Q}_{s,p}\left(\frac{\nu}{\nu_0}\right)^{\beta_{s,p}+2}$$

Martínez-Solaeche et al. 2018

$$Q^{\mathrm{MKD}}_{\nu,p} = \sum_{l=1}^{6} A^{Q}_{d,l,p}\left(\frac{\nu}{\nu_0}\right)^{\beta_{d,l,p}} B_\nu(T_{d,l,p})$$

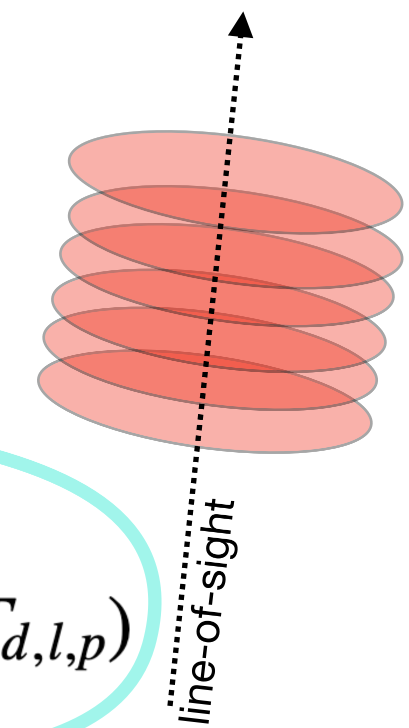

“the parameters describing the frequency scaling of the dust emission vary across the sky, they must also vary along the line of sight.“

Draine & Hensley 2013

$$\log_{10}\mathcal{U}_p = (4 + \beta_{d,p})\log_{10}\left(\frac{T_{d,p}}{\langle T_d\rangle}\right)$$

$$Q^{\mathrm{d7}}_{\nu,p} = A^{Q}_{d,p}\,\frac{f_\nu(\mathcal{U}_p)}{f_{\nu_0}(\mathcal{U}_p)}$$

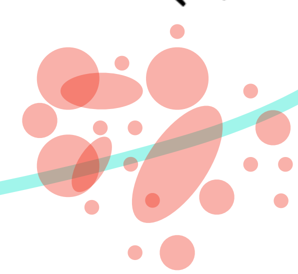

“ […] the dust emission is modeled as arising from a population of dust grains with different compositions, sizes, and temperatures, as described by Hensley (2015).”

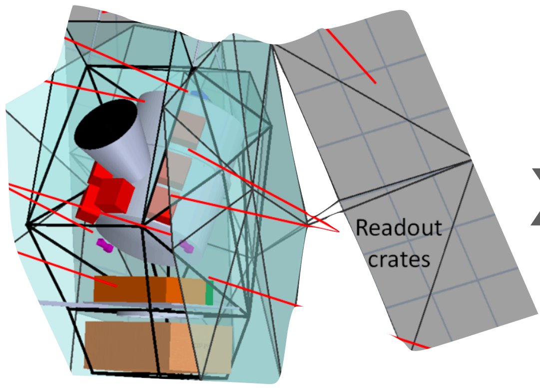

x

sky simulations

CMB + noise + galactic foregrounds

x 10

d1s1 d7s3 MKD

Zonca et al. 2021

$$Q^{\mathrm{d1}}_{\nu,p} = A^{Q}_{d,p}\left(\frac{\nu}{\nu_0}\right)^{\beta_{d,p}} B_\nu(T_{d,p})$$

$$Q^{\mathrm{s1}}_{\nu,p} = A^{Q}_{s,p}\left(\frac{\nu}{\nu_0}\right)^{\beta_{s,p}+2}$$

Martínez-Solaeche et al. 2018

$$Q^{\mathrm{MKD}}_{\nu,p} = \sum_{l=1}^{6} A^{Q}_{d,l,p}\left(\frac{\nu}{\nu_0}\right)^{\beta_{d,l,p}} B_\nu(T_{d,l,p})$$

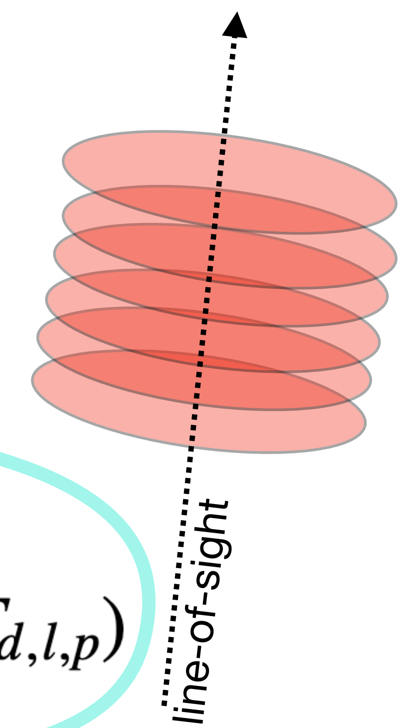

"the parameters describing the frequency scaling of the dust emission vary across the sky, they must also vary along the line of sight."

Draine & Hensley 2013

$$\log_{10}\mathcal{U}_p = (4 + \beta_{d,p})\log_{10}\left(\frac{T_{d,p}}{\langle T_d\rangle}\right)$$

$$Q^{\mathrm{d7}}_{\nu,p} = A^{Q}_{d,p}\frac{f_\nu(\mathcal{U}_p)}{f_{\nu_0}(\mathcal{U}_p)}$$

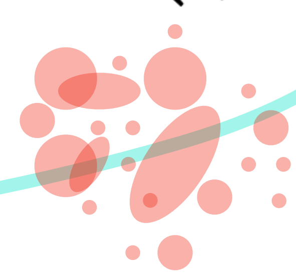

" [...] the dust emission is modeled as arising from a population of dust grains with different compositions, sizes, and temperatures, as described by Hensley (2015)."

same for Stokes **U**

beam conv. **foregrounds** **CMB** **noise**

$$Q_{\nu,p} = G_\nu \star (Q^{\mathrm{fgs}}_{\nu,p} + Q^{\mathrm{CMB}}_{\nu,p}) + n_{\nu,p}$$

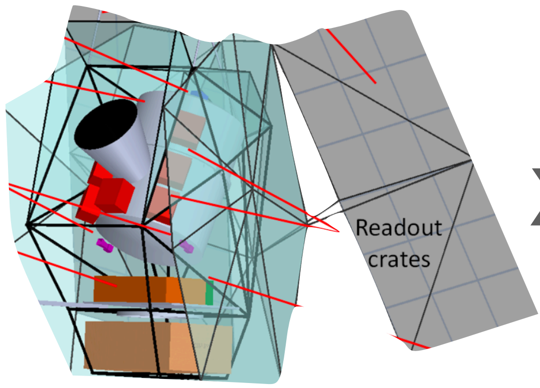

X

sky simulations

CMB + noise + galactic foregrounds

x 10

d1s1 d7s3 MKD

Zonca et al. 2021

$$Q^{\mathrm{d1}}_{\nu,p} = A^{Q}_{d,p}\left(\frac{\nu}{\nu_0}\right)^{\beta_{d,p}} B_\nu(T_{d,p})$$

$$Q^{\mathrm{s1}}_{\nu,p} = A^{Q}_{s,p}\left(\frac{\nu}{\nu_0}\right)^{\beta_{s,p}}$$

Martínez-Solaeche et al. 2018

$$Q^{\mathrm{MKD}}_{\nu,p} = \sum_{l=1}^{6} A^{Q}_{d,l,p}\left(\frac{\nu}{\nu_0}\right)^{\beta_{d,l,p}} B_\nu(T_{d,l,p})$$

foregrounds complexity ↗

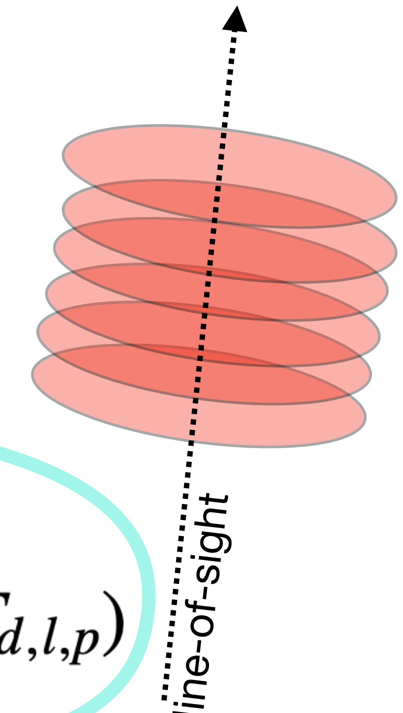

"the parameters describing the frequency scaling of the dust emission vary across the sky, they must also vary along the line of sight."

Draine & Hensley 2013

$$\log_{10}\mathcal{U}_p = (4+\beta_{d,p})\log_{10}\left(\frac{T_{d,p}}{\langle T_d\rangle}\right)$$

$$Q^{\mathrm{d7}}_{\nu,p} = A^{Q}_{d,p}\frac{f_\nu(\mathcal{U}_p)}{f_{\nu_0}(\mathcal{U}_p)}$$

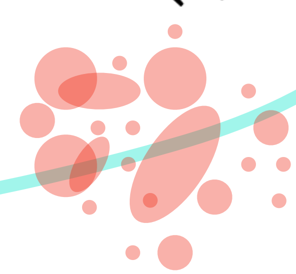

" [...] the dust emission is modeled as arising from a population of dust grains with different compositions, sizes, and temperatures, as described by Hensley (2015)."

same for Stokes **U**

beam conv. **foregrounds** **CMB** **noise**

$$Q_{\nu,p} = G_\nu \star (Q^{\mathrm{fgs}}_{\nu,p} + Q^{\mathrm{CMB}}_{\nu,p}) + n_{\nu,p}$$

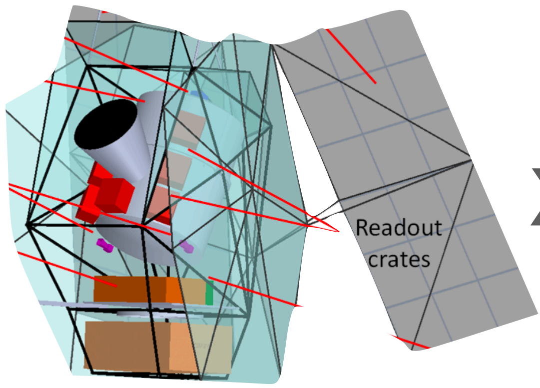

X

sky simulations

CMB + noise + galactic foregrounds

x 10

d1s1 d7s3 MKD

component separation

- harmonic
- blind/non-parametric

NILC fgbuster

- parametric
- pixel-based

$$\boldsymbol{d}_p = \boldsymbol{a} c_p + \boldsymbol{A}_p \boldsymbol{f}_p + \boldsymbol{n}_p$$

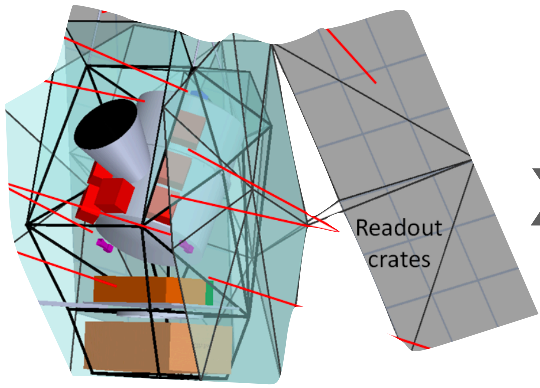

X

sky simulations

CMB + noise + galactic foregrounds

x 10

d1s1 | d7s3 | MKD

component separation

NILC | fgbuster

$$\boldsymbol{d}_p = \boldsymbol{a} c_p + \boldsymbol{A}_p \boldsymbol{f}_p + \boldsymbol{n}_p$$

$$\hat{s}_p^{(j)} = \sum_\nu w_{\nu,p}^{(j)} \, d_{\nu,p}^{(j)}$$

$$\boldsymbol{w}_p^{(j)} = \frac{\boldsymbol{a}^{\mathrm{T}} [\boldsymbol{C}_p^{(j)}]^{-1}}{\boldsymbol{a}^{\mathrm{T}} [\boldsymbol{C}_p^{(j)}]^{-1} \boldsymbol{a}}$$

$$\mathrm{C}_{p,\nu\nu'}^{(j)} = \int dp' W_{p,p'}^{(j)} d_{\nu,p'}^{(j)} d_{\nu',p'}^{(j)}$$

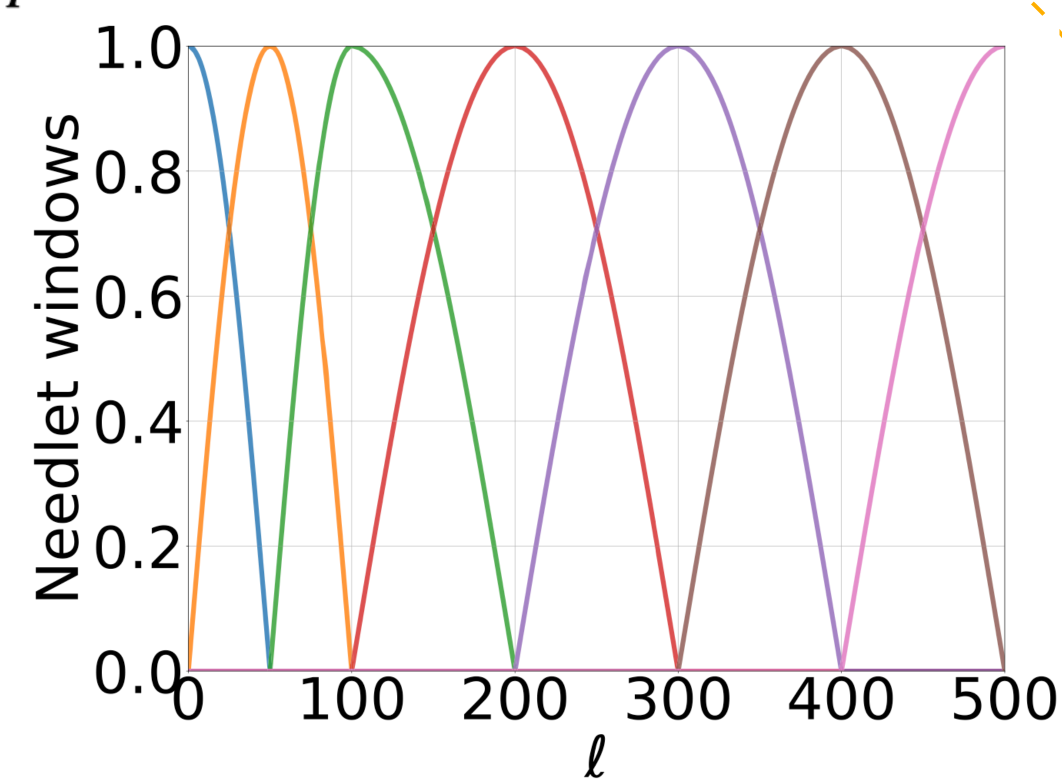

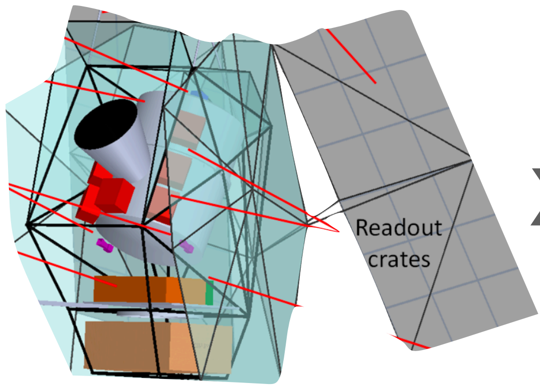

x

x 10

sky simulations

CMB + noise + galactic foregrounds

d1s1 d7s3 MKD

component separation

NILC fgbuster

$$\boldsymbol{d}_p = \boldsymbol{a} c_p + \boldsymbol{A}_p \boldsymbol{f}_p + \boldsymbol{n}_p$$

$$\boldsymbol{d}_p = \left[\boldsymbol{a}\ \boldsymbol{A}_p\right]\begin{bmatrix} c_p \\ \boldsymbol{f}_p \end{bmatrix} + \boldsymbol{n}_p \equiv \boldsymbol{\Lambda}_p \boldsymbol{s}_p + \boldsymbol{n}_p$$

assuming **2 modified black bodies** ($\beta_d^{(1)}$, $T_d^{(1)}$, $\beta_d^{(2)}$ free, $T_d^{(2)}$=20K) + **synchrotron** (β_s =-3 fixed)

spectral likelihood

$$-2\log(\mathcal{L})(\beta) = -\sum(\hat{\boldsymbol{d}}^T N^{-1}\boldsymbol{\Lambda})(\boldsymbol{\Lambda}^T N^{-1}\boldsymbol{\Lambda})^{-1}(\boldsymbol{\Lambda}^T N^{-1}\hat{\boldsymbol{d}})$$

foreground-cleaned CMB

$$\tilde{\boldsymbol{s}} = (\tilde{\boldsymbol{\Lambda}}^T N^{-1}\tilde{\boldsymbol{\Lambda}})^{-1}\tilde{\boldsymbol{\Lambda}}^T N^{-1}\hat{\boldsymbol{d}}$$

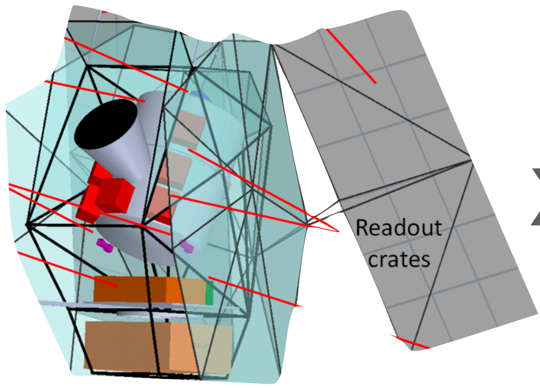

X

x 10

sky simulations

CMB + noise + galactic foregrounds

d1s1 | d7s3 | MKD

↓ ↓ ↓

component separation

NILC | fgbuster

↓ ↓

cosmological analysis, $\mathcal{L}(\tau)$

→ $\tau \pm$ 68% c.l. $\sigma(\tau)$

$$-2\ln\mathcal{L}(\tau) = \sum_{\ell}(2\ell+1)f_{\rm sky}\left[\frac{\widehat{C}_{\ell}^{\rm EE}}{C_{\ell}^{\rm EE,theory}(\tau)+\widehat{N}_{\ell}} + \ln\left(C_{\ell}^{\rm EE,theory}(\tau)+\widehat{N}_{\ell}\right)\right]$$

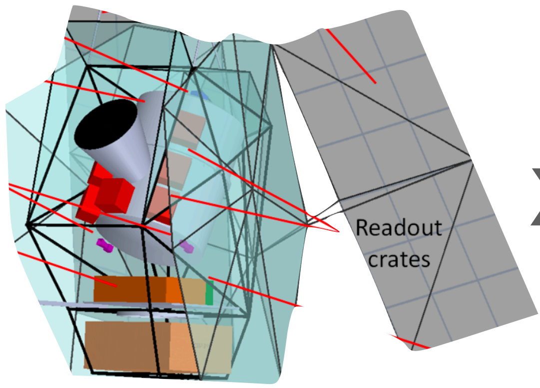

x

x 10

sky simulations

CMB + noise + galactic foregrounds

d1s1 | d7s3 | MKD

- removing / adding high frequencies
- changing fsky
- considering or not synchrotron in the analysis

component separation

NILC | fgbuster

cosmological analysis, $\mathcal{L}(\tau)$

$\tau \pm$ 68% c.l. $\sigma(\tau)$

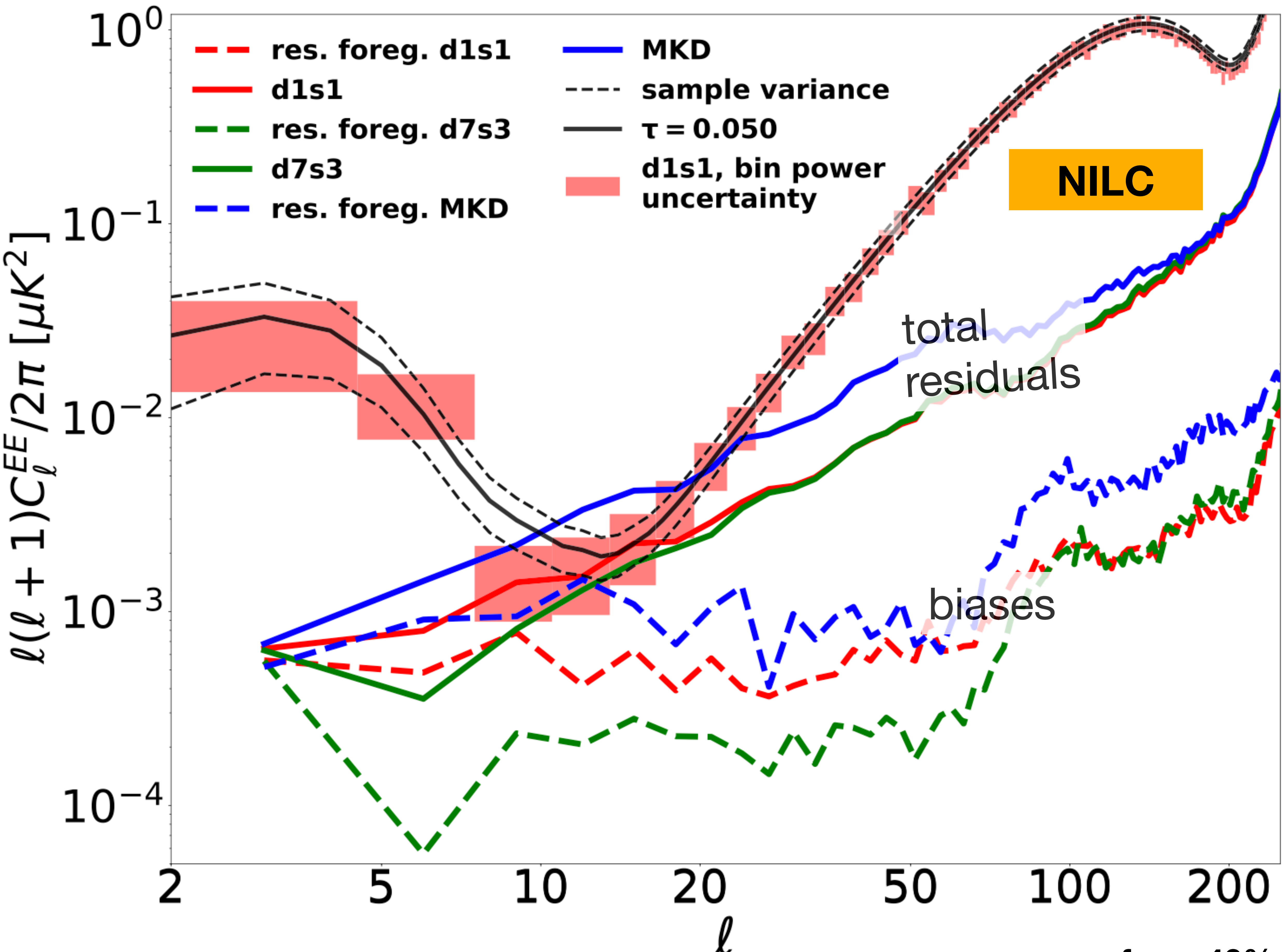

res. foreg. d1s1
d1s1
res. foreg. d7s3
d7s3
res. foreg. MKD
MKD
sample variance
τ = 0.050
d1s1, bin power uncertainty
NILC
total residuals
biases
$\ell(\ell+1)C_\ell^{EE}/2\pi\ [\mu K^2]$
ℓ
10^0
10^{-1}
10^{-2}
10^{-3}
10^{-4}
2
5
10
20
50
100
200

f_{sky} = 40%

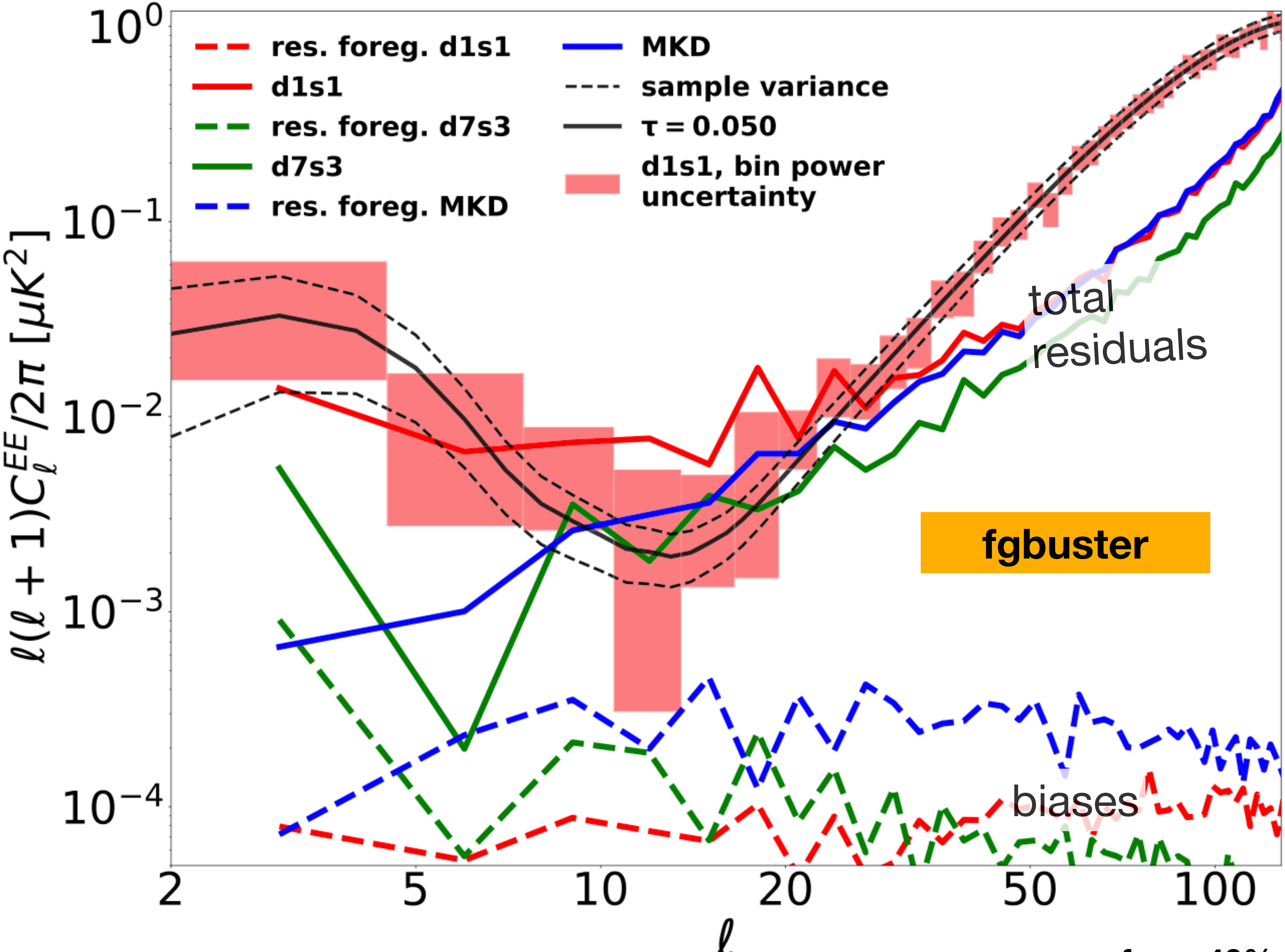
res. foreg. d1s1
d1s1
res. foreg. d7s3
d7s3
res. foreg. MKD
MKD
sample variance
τ = 0.050
d1s1, bin power uncertainty
$\ell(\ell+1)C_\ell^{EE}/2\pi\ [\mu K^2]$
ℓ
10^0
10^{-1}
10^{-2}
10^{-3}
10^{-4}
2
5
10
20
50
100
total residuals
fgbuster
biases

f_{sky} = 40%

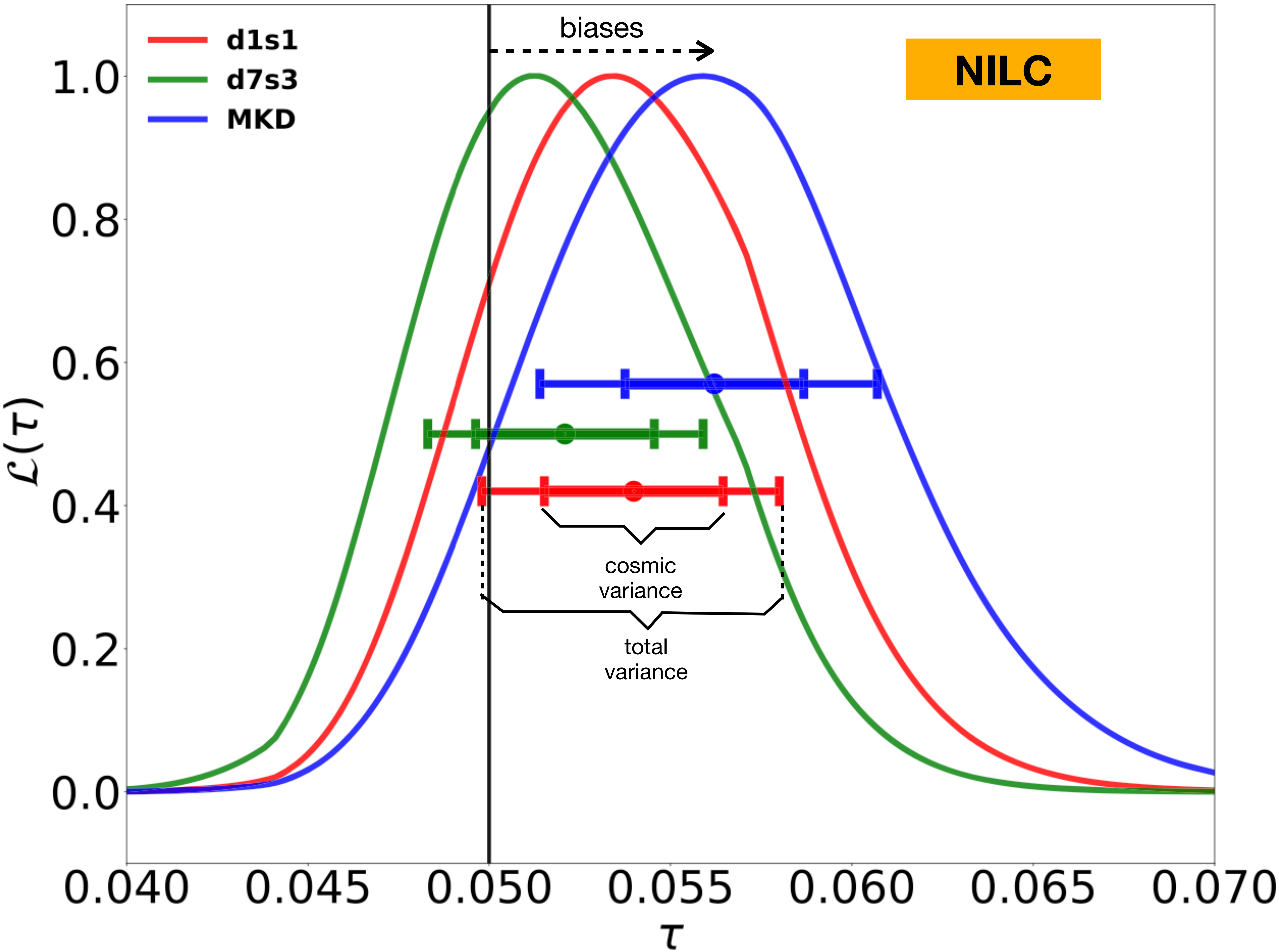

biases
d1s1
d7s3
MKD
NILC
1.0
0.8
0.6
0.4
0.2
0.0
$\mathcal{L}(\tau)$
cosmic variance
total variance
0.040
0.045
0.050
0.055
0.060
0.065
0.070
τ

f_{sky} = 40%

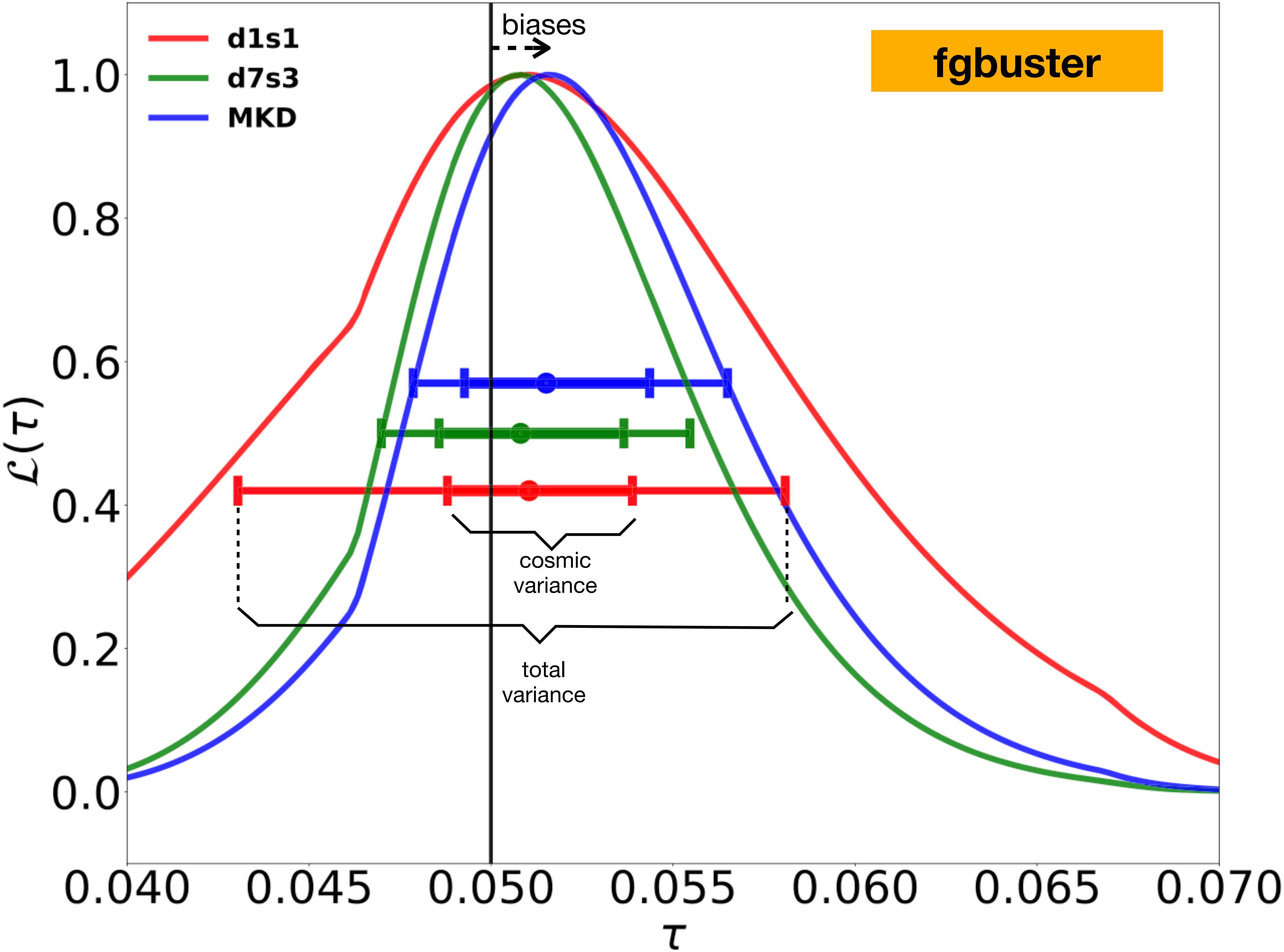

biases
d1s1
d7s3
MKD
fgbuster
1.0
0.8
0.6
0.4
0.2
0.0
$\mathcal{L}(\tau)$
cosmic variance
total variance
0.040
0.045
0.050
0.055
0.060
0.065
0.070
τ

f_{sky} = 40%

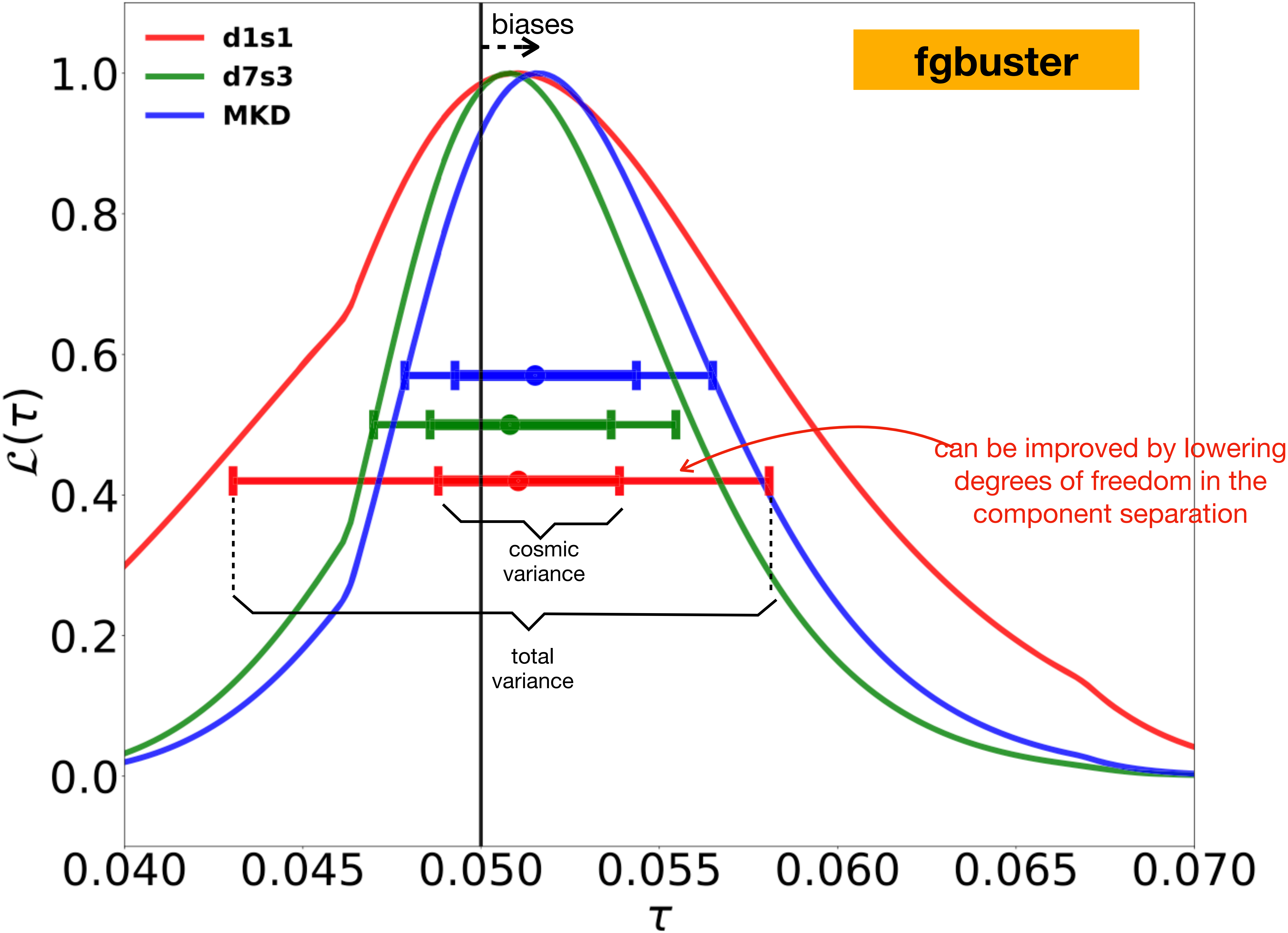
biases
fgbuster
d1s1
d7s3
MKD
1.0
0.8
0.6
0.4
0.2
0.0
$\mathcal{L}(\tau)$
can be improved by lowering degrees of freedom in the component separation
cosmic variance
total variance
0.040
0.045
0.050
0.055
0.060
0.065
0.070
τ

f_{sky} = 40%

	d1s1	d7s3	MKD
NILC			
τS	0.0540 ± 0.0041	0.0521 ± 0.0038	0.0562 ± 0.0046
τS-lf	0.0534 ± 0.0049	0.0529 ± 0.0049	0.0563 ± 0.0064
fgbuster	d1s1	d7s3	MKD
τS[a]	0.0506 ± 0.0044	0.0508 ± 0.0047	0.0515 ± 0.0050
$\chi^2_{\tau S}$	0.999 ± 0.004	0.999 ± 0.004	0.999 ± 0.004
min/max PTE	0.13/0.96	0.11/0.96	0.12/0.96
τS-lf[b]	0.0512 ± 0.0076	0.0540 ± 0.0063	0.0525 ± 0.0089
$\chi^2_{\tau S-\mathrm{lf}}$	0.998 ± 0.006	0.998 ± 0.006	0.998 ± 0.006
min/max PTE	0.08/0.98	0.07/0.97	0.08/0.97

- removing the 2 highest frequency bands leads to an **increase of σ(τ)** but also an **increase of the bias**
  ➔ one of the benefits from balloon-borne experiments
- adding 2 more frequency bands > 400GHz does not tighten constraint on τ.

Name	Short Description	d1s1	d7s3	MKD
		NILC		
τS (no 30/44)	Not using 30 and 44 GHz data	0.0671 ± 0.0056	0.0620 ± 0.0052	0.0703 ± 0.0057
τS-hf	+450 and 600 GHz	0.0528 ± 0.0041	0.0521 ± 0.0038	0.0558 ± 0.0046
τS (noise $\times 0.1$)	Lower noise by $\times 10$	0.0534 ± 0.0037	0.0523 ± 0.0033	0.0556 ± 0.0039
τS-80%	$f_{\rm sky} = 80\%$	0.0540 ± 0.0029	0.0520 ± 0.0027	0.0600 ± 0.0035
		fgbuster		
τS (dust+cmb)	Only fit for dust + CMB	0.097 ± 0.0071	0.136 ± 0.0051	0.115 ± 0.0060
τS (no 30/44)	Not using 30 and 44 GHz data	0.0530 ± 0.026	0.0518 ± 0.035	0.0545 ± 0.050
τS-hf	+450 and 600 GHz	0.0510 ± 0.0034	0.147 ± 0.0055	0.374 ± 0.0070
χ^2 (τS-hf)		1.0003 ± 0.0022	1.0034 ± 0.0021	29.4 ± 0.8
min/max PTE		0.09/0.81	0.01/0.36	0/0
τS (noise $\times 0.1$)	Lower noise by $\times 10$	0.0503 ± 0.0031	0.0508 ± 0.0031	0.0513 ± 0.0032
τS-80%	$f_{\rm sky} = 80\%$	0.0515 ± 0.0029	0.0506 ± 0.0024	0.0550 ± 0.0037

Note. For fgbuster and τS-hf, we include the average χ^2 values, comparing the input and inferred sky signals and the range of PTEs. For all cases except τS-80%, $f_{\rm sky} = 40\%$. The confidence limits are 68% intervals.

- forgetting about synchrotron in the analysis leads to several σ biases on τ.
- A North+South τS flights could potentially lead to $\sigma(\tau) < 0.003$

- increasing f_{sky} decreases $\sigma(\tau)$ but biases could quickly become significant

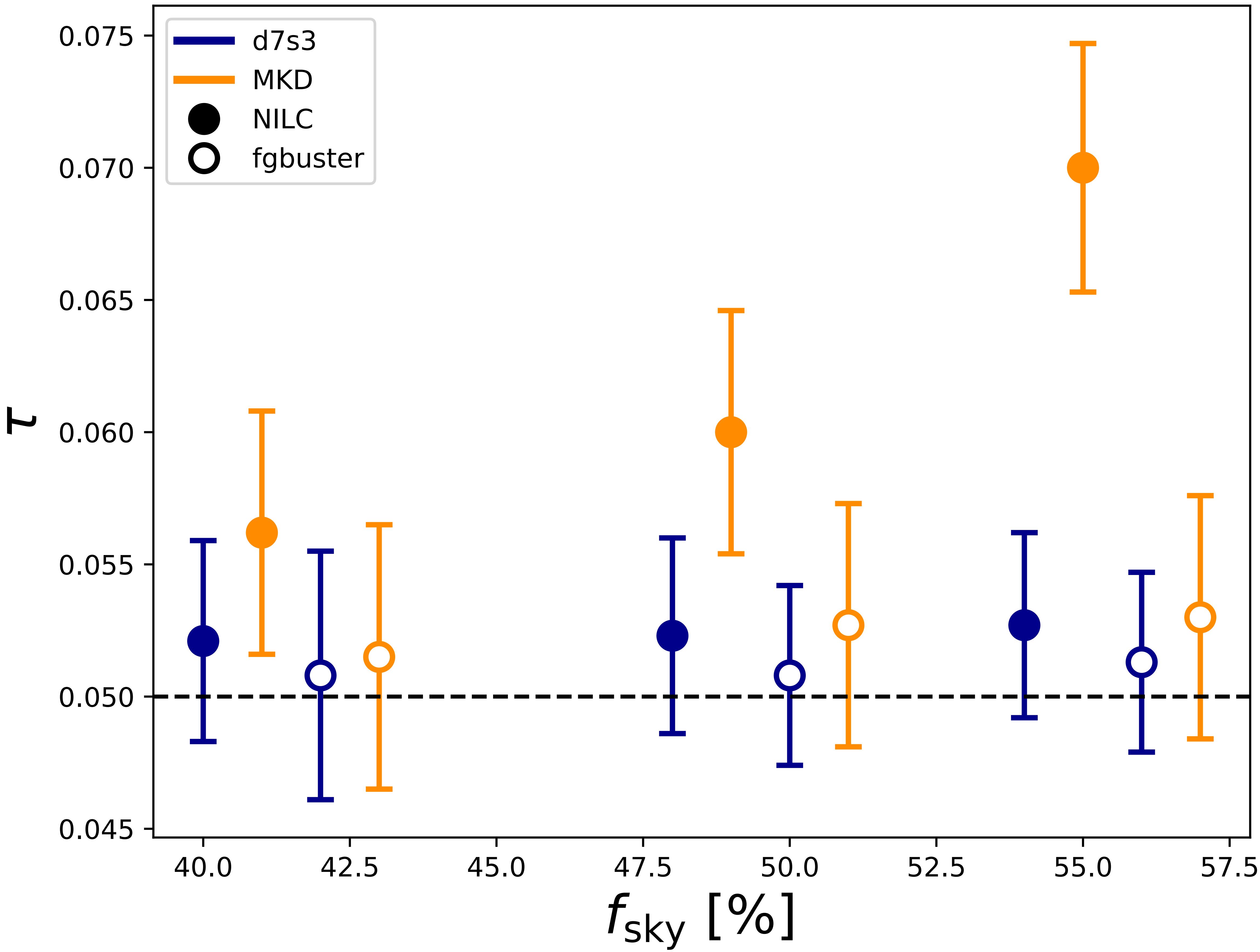

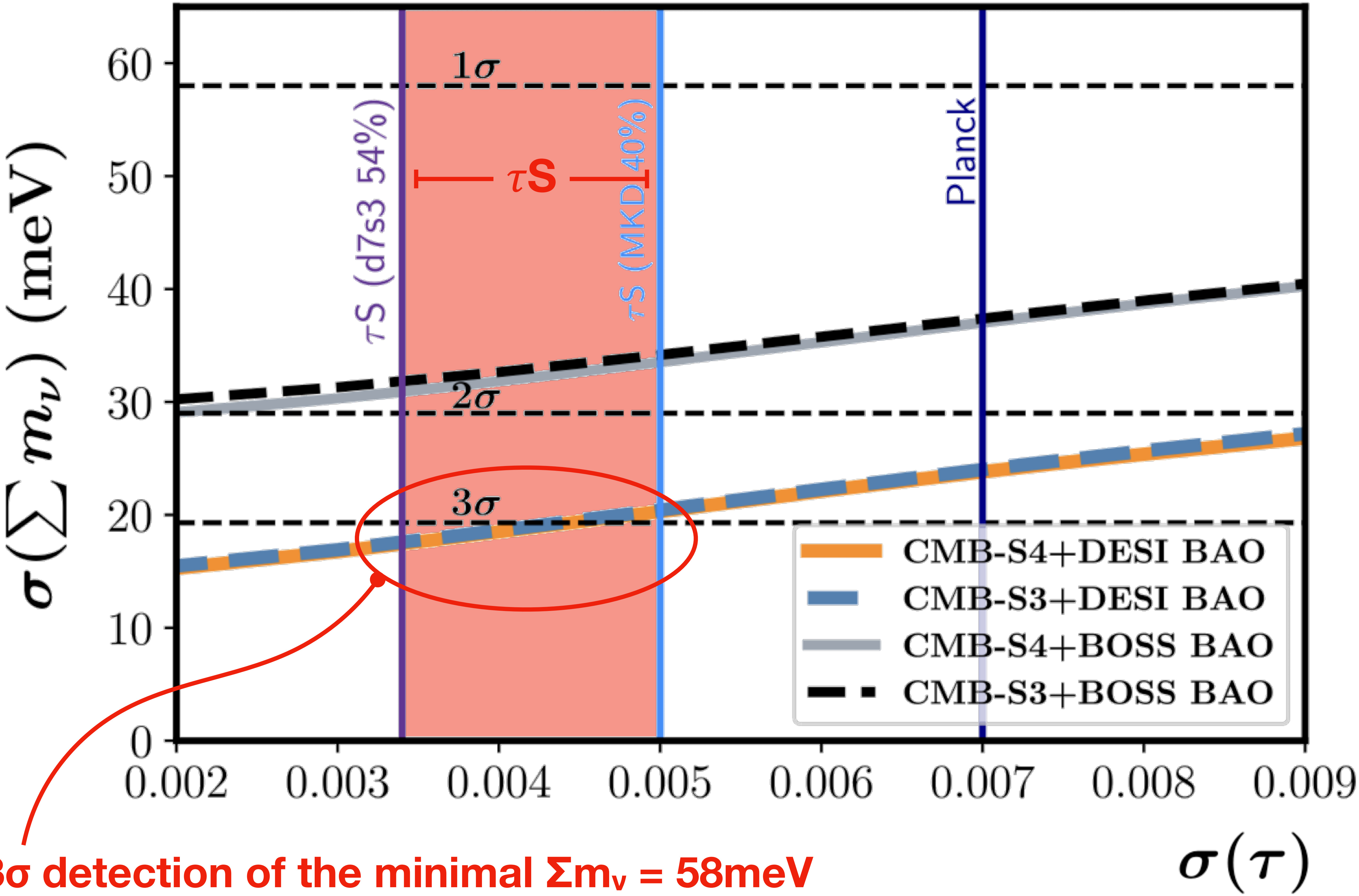

3σ detection of the minimal Σm_ν = 58meV

⚠️ **MKD foregrounds**

⚠️ **removal of the hightest frequency bands**

	$\beta_d^{(1)}$	$T_d^{(1)}$	$\beta_d^{(2)}$	$T_d^{(2)}$	β_s
1 MBB/1 dof	✓	…	…	…	…
1 MBB/2 dof	✓	✓	…	…	…
1 MBB/3 dof	✓	✓	…	…	✓
2 MBBs/3 dof	✓	✓	✓	…	…
2 MBBs/4 dof	✓	✓	✓	✓	…
2 MBBs/5 dof	✓	✓	✓	✓	✓

- bias on τ goes down with an increasing number of dof (in the component separation)
- error bars go up with an increasing number of dof
- optimal tradeoff, in the particular case of τ**S**, is for 2MBB and 3 dof.

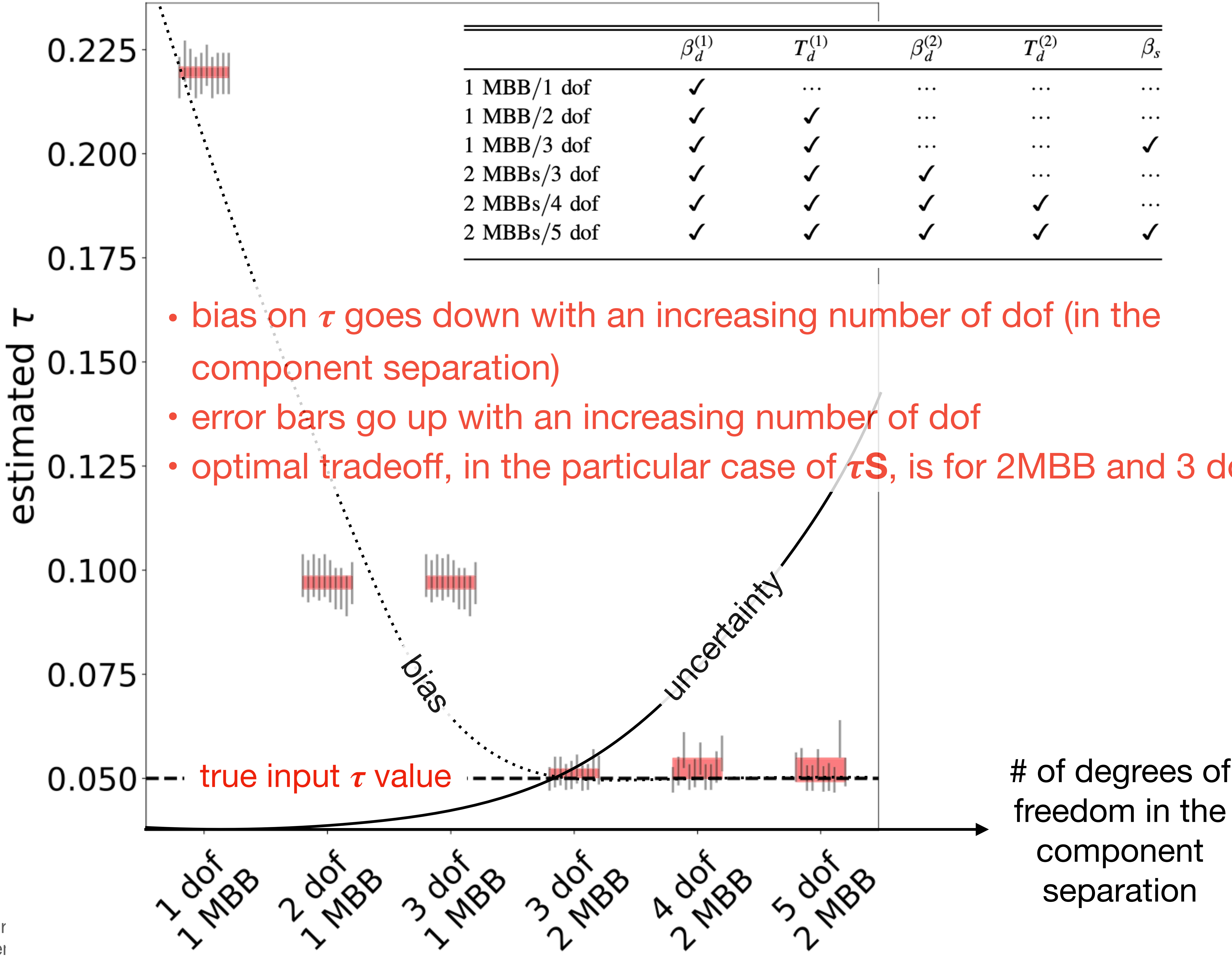

Conclusions

- 2 frequency bands > 300GHz lead to a 20-60% smaller σ(τ) relative to a configuration without them;
- adding 2 more frequency bands > 400GHz does not tighten constraint on τ;
- only under the most optimistic assumptions the balloon achieves a 3σ detection of the minimal sum of neutrino masses (58meV), when combined with CMB lensing and DESI BAO;
- synchrotron emission cannot be neglected;
- a τS-like instrument would give only mild improvement on τ constraints under the MKD foreground;
- increasing f_{sky} decreases σ(τ) but biases could quickly become significant;
- North+South τS flights could potentially lead to σ(τ) < 0.003 over f_{sky} =80%.

➔ more details at https://arxiv.org/abs/2206.03389

Science from
the large scale cosmic
microwave background
polarization structure

European Research Council
Established by the European Commission

PhD, PostDoc and software engineer positions to be filled this year!

➔ contact me if interested: josquin@apc.in2p3.fr

➔ more info at scipol.in2p3.fr